Chemogenetic activation of noradrenergic A5 neurons increases blood pressure and visceral sympathetic activity in adult rats

Souza, George M P R ; Stornetta, Daniel S ; Vitali, Alexander J ; Wildner, Hendrik ; Zeilhofer, Hanns Ulrich ; Campbell, John N ; Abbott, Stephen B G

DOI: https://doi.org/10.1152/ajpregu.00119.2022

Chemogenetic activation of noradrenergic A5 neurons increases blood pressure and visceral sympathetic activity in adult rats.

Running title: A5 and the sympathetic control of blood pressure

George M. P. R. Souza [1], Daniel S. Stornetta [1], Alexander J. Vitali [1], Hendrik Wildner [3,4], Hanns U. Zeilhofer [3,4], John N. Campbell [2], and Stephen B. G. Abbott [1]

1. Department of Pharmacology, University of Virginia, Charlottesville, VA
2. Department of Biology, University of Virginia, Charlottesville, VA
3. Institute of Pharmacology and Toxicology, University of Zurich, Winterthurerstrasse 190, 8057, Zurich, Switzerland
4. Institute of Pharmaceutical Sciences, Swiss Federal Institute of Technology (ETH) Zurich, Vladimir-Prelog-Weg 1-5/10, 8090, Zurich, Switzerland

Correspondence to:

Stephen B.G. Abbott

Department of Pharmacology, University of Virginia

1340 Jefferson Park Avenue, Charlottesville, VA, 22908

e-mail: sba6t@virginia.edu

Author contributions: S.B.G.A., J.N.C. and G.M.P.R.S. designed the research, S.B.G.A. and G.M.P.R.S. conducted all the physiological experiments and data analysis, D.S.S. performed histological

preparations, S.B.G.A. and A.V. analyzed histology, H.W. and H.U.Z generate unpublished reagents, S.B.G.A, G.M.P.R.S., D.S.S. wrote the paper and approved the final version of the manuscript.

Funding: This work was supported by an American Heart Association grant (19POST34430205) to G.M.P.R.S. and by National Institute of Health grant HL148004 to S.B.G.A.

Conflict of interest: The authors declare no competing interests.

Abstract

In mammals, the pontine noradrenergic system influences nearly every aspect of central nervous system function. A subpopulation of pontine noradrenergic neurons, called A5, are thought to be important in the cardiovascular response to physical stressors, yet their function is poorly defined. We hypothesized that activation of A5 neurons stimulates a sympathetically-mediated increase in BP. To test this hypothesis, we conducted a comprehensive assessment of the cardiovascular effects of chemogenetic stimulation of A5 neurons in male and female adult rats using intersectional genetic and anatomical targeting approaches. Chemogenetic stimulation of A5 neurons in freely behaving rats elevated BP by 15 mmHg and increased cardiac baroreflex sensitivity with a negligible effect on resting HR. Importantly, A5 stimulation had no detectable effect on locomotor activity, metabolic rate or respiration. Under anesthesia, stimulation of A5 neurons produced a marked elevation in visceral sympathetic nerve activity (SNA) and no change in skeletal muscle SNA, showing that A5 neurons preferentially stimulate visceral SNA. Interestingly, projection mapping indicates that A5 neurons target sympathetic preganglionic neurons throughout the spinal cord and parasympathetic preganglionic neurons throughout in the brainstem, as well as the nucleus of the solitary tract, and ventrolateral medulla. Moreover, *in situ* hybridization and immunohistochemistry indicate that a sub-population of A5 neurons co-release glutamate and monoamines. Collectively, this study suggests A5 neurons are a central modulator of

autonomic function with a potentially important role in sympathetically-driven redistribution of blood flow from the visceral circulation to critical organs and skeletal muscle.

Introduction

The pontine noradrenergic system influences nearly every aspect of CNS function (1). In rodents, the pontine noradrenergic system has been subdivided into 3 groups, A5, A6, and A7 (2), with A5 neurons forming a discrete population of noradrenergic cells embedded within the ventrolateral pontine tegmentum. Based on anatomical and functional evidence in rats, A5 neurons are a significant source of noradrenergic input to sympathetic preganglionic neurons (SPN) in the spinal cord (3-6). Electrophysiological recordings and studies using cFOS as a marker of neuronal activation indicate that A5 neurons are uniformly activated by hypoxia and stimulation of the peripheral chemoreceptors (7-11), and many (~60%) are modulated by changes in BP (9, 12-14). Consequently, A5 neurons are thought to contribute to the sympathetic regulation of cardiovascular function.

The role of A5 neurons in blood pressure (BP) regulation is a matter of ongoing debate stemming from discrepancies in the effect of activating these neurons (4, 15-20). Previous work indicates that A5 neurons drive a complex cardiovascular response involving visceral vasoconstriction and skeletal muscle vasodilatation that results in a decrease or no change in BP. However, a limitation of the existing literature is the reliance on indiscriminant methods for neuronal stimulation. When A5 neurons have been genetically targeted for optogenetic stimulation in anesthetized rats, no change in BP was observed, with only a short-latency burst in renal and lumbar sympathetic nerve activity (SNA) attributed to the release of an unidentified fast neurotransmitter (9). This evidence suggests that A5 neurons stimulate visceral SNA and to a lesser extent skeletal muscle SNA, but this is insufficient to increase BP. Further complicating the matter, noradrenaline is known to both excite and inhibit SPN(21-25), and intrathecal administration of noradrenaline in anesthetized rats inhibits renal SNA at low concentrations, and excites renal SNA at high doses (26). Hence, the sympathetic and cardiovascular effects of A5 stimulation may reflect not only contrasting responses of visceral and skeletal muscle sympathetic nerves that are

influenced by experimental conditions, such as the use of anesthesia, but also the summation of excitation and inhibition of SPN mediated by distinct adrenoreceptor signaling pathways.

To build a consensus for the function of A5 neurons in the sympathetic control of BP, we conducted chemogenetic stimulation of A5 neurons in adult rats using Designer Receptors Exclusively Activated by Designer Drugs (DREADDs) targeted with complementary genetic and anatomical approaches. We hypothesized that selective stimulation of A5 neurons in freely behaving rats would be sufficient to increase BP, which was tested with an assessment of the cardiovascular, respiratory and metabolic effects of A5 stimulation. Furthermore, we predicted A5 stimulation would evoke differential effects on visceral and skeletal muscle SNA based on previous functional studies (4, 9, 20), which we tested by measuring the effects of selective A5 stimulation on splanchnic and lumbar SNA under anesthesia. Finally, we assessed the neurochemical profile of A5 neurons and their projections to cardiovascular centers in the brainstem and spinal cord to shed light on the neural network that mediates the effects of A5 stimulation.

Methods

Ethics Approval

All experiments were conducted in accordance with the National Institutes of Health's Guide for the Care and Use of Laboratory Animals and approved by the University of Virginia Animal Care and Use Committee (protocol #4312).

Animals

Studies were conducted using adult male (n=33) and female (n=38) rats. Outbred Sprague-Dawley rats were acquired from Taconic (NTac:SD) and *Th-cre* (SD-TH$^{tm1(IRES\text{-}cre)\ Sage}$, TGRA8400; RRID: RGD_12905029; Sprague-Dawley background) were acquired from Envigo RMS and bred in-house. *Th-cre* rats have a targeted insertion of IRES-Cre immediately after the translational stop in the open reading

frame of *Th*. Rats weighed 120-300 g at the time of virus microinjections and 200-600 g during experiments. Animals were group housed before injections and during recovery from surgery under 12:12 light: dark cycle (lights on 7 am) at 23°C-24°C with water and food provided *ad libitum*.

Viruses

AAV_2-hSyn-DIO-hM3D(Gq)-mCherry (Addgene plasmid 44361, titer for injection: 8.0 x 10^{11} GC/mL). AAV_8- hSyn-(cre^{ON}/$flpo^{ON}$)-HM3Dq-HA (serotype 8; titer for injection: 8.0 x 10^{11} GC/mL, produced by H.W. and H.U.Z.). AAV-hSyn-DIO-mCherry (serotype 5; Addgene plasmid 50459, titer for injection: 8.0 x 10^{11} GC/mL). LV-PRSx8-cre (Salk Institute, La Jolla, CA, titer for injection: 4.0 x 10^9 TU/mL). PRSx8 is a binding site for Phox2a or b and drives transgene expression selectively in neurons that express high levels of one or both of these transcription factors (Hwang et al., 2001). AAV_{rg}-hSyn-cre (Addgene plasmid 105555, titer for injection: 1.5 x 10^{13} GC/mL). AAV_{rg}-EF1a-Flpo (Addgene plasmid 55637, titer for injection: 1.3 x 10^{13} GC/mL)). AAV_{DJ}-hSyn FLEX-mGFP-2A-synaptophysin-mRuby (item code: GVVC-AAV-101, Wu Tsai Neurosciences Institute, Gene Vector and Virus Core, Stanford, titer for injection: 4 x 10^{12} TU/mL))

AAV and CTB Microinjections

Rats were anesthetized with a mixture of ketamine (75 mg/kg), xylazine (5 mg/kg), and acepromazine (1 mg/kg, i.m.). The depth of anesthesia was assessed by the absence of a withdrawal reflex to a firm tail or hind paw pinch and by monitoring breathing rate. Surgical procedures were conducted under aseptic conditions. Additional anesthetic was administered if required (25% of the original dose, i.m.). Core temperature was maintained at 37°C with a servo-controlled heating pad. Analgesic (ketoprofen, 3-5 mg/kg, s.c.) was administered each day for 3 days following surgery.

Microinjections in the A5 region were performed in a stereotaxic frame with the bite bar set at -3.5 mm below the interaural line for a flat skull and the micromanipulator angle set to 12-15 degrees off vertical

in the anterior direction. Virus was microinjected using glass capillaries (1.2 mm O.D. 0.64 mm I.D., pulled to a tip size of 40 µm) in 3 sites bilaterally (AP: -8.4 mm, -8.0 mm, -7.7 mm from bregma; ML: ±2.2 mm of midline; DV: -8.6 mm of brain surface) with a volume of 60-150 nL per site.

Microinjections in the spinal cord were performed in a stereotaxic frame with the bite bar set at 0.0 mm below the interaural line and a vertical micromanipulator. Following a dorsal midline incision, the brown adipose tissue was dissected and retracted. Tissue overlying the T3 vertebra was cleared and the dorsal surface of the vertebra was removed using rongeurs. The dura was split using a sterile needle exposing the spinal cord. Virus or Cholera Toxin B Subunit (Choleragenoid) from Vibrio cholerae (CTB, 0.5% in sterile water, List Biological Cat# 104, RRID:AB_2313636) was microinjected using glass capillaries (1.2 mm O.D. 0.64 mm I.D., pulled to a tip size of 20 µm) in 2 bilateral locations separated by 1 mm along the rostro-caudal axis (4 sites in total, ML: 0.8 mm of lateral of midline; DV: 1.1 to 1.3 mm ventral of spinal cord surface) with a volume of 150 nL per site for AAV, and 50 nL per site for CTB. Following microinjections, Internal wounds were closed with absorbable sutures, while external wounds were made with steel surgical clips and veterinary adhesive.

BP recordings and analysis

Three to five weeks after microinjections, rats were re-anesthetized with 2.5% isoflurane in oxygen and a radiotelemetry probe (PA-C10; Data Sciences International) was implanted in the femoral artery. Following a minimum of 7 days recovery, pulsatile arterial pressure and locomotor activity was acquired at 500 Hz and 50 Hz respectively with a CED 1401 A/D acquisition system using Spike2 (Version 8 & 9, Cambridge Electronic Design, UK).

Animals were singly housed during experiments in standard rat cages (45cm x 30cm x 20 cm) under 12:12 light: dark cycle (lights on 7am) at 23°C-24°C with water and food provided *ad libitum*. Clozapine-N-oxide (0.03 – 1.0 mg/kg, 0.5 mg/mL in physiological saline, Sigma product id C0832), C21 dihydrochloride (1.0 mg/kg, 0.5 mg/mL in physiological saline, Tocris product id 6422) or vehicle was

administered intraperitoneally in randomized order during the light phase (0900-1200 hours) or dark phase (2100-2200 hours) with at least 48 hrs. between injections.

Mean arterial pressure (MAP), heart rate (HR) and pulse pressure was derived from pulsatile arterial pressure using a publicly available script (HRBP8 script from Cambridge Electronic Design, UK, www.ced.co.uk/downloads/scriptspkanal). For analysis of cardiovascular parameters, mean values over a 10 s period were extracted in 15 minute intervals for 4 hours after drug administration. Statistical comparisons of the change in MAP, HR and pulse pressure between groups were based on the average of data points 120-150 minutes after drug administration, which is where the MAP increase plateaued. Spectral analysis of HR and spontaneous baroreflex sensitivity (sBRS) was analyzed using CardioSeries v2.7 (www.danielpenteado.com). Systolic BP (SBP) and pulse interval (PI) signals were derived from a 30 min segment of arterial BP data 120-150 minutes after drug administration. The variability of HR was calculated in the time domain and expressed as variance (σ). HR spectra was calculated using a fast Fourier transform and expressed as low frequency power (LF, 0.2-0.75 Hz) and high frequency power (HF, 0.75-3.0 Hz). The LF/HF ratio was used as a measure of sympathovagal balance. The spontaneous baroreflex (sBRS) was analyzed using the sequence method. Sequences of 4 or more consecutive increases or decreases in SBP were plotted against corresponding PI values (lag = 0). sBRS was derived from the mean slope of sequences with a linear correlation between SBP and PI greater than 0.8 (range: 7-112 sequences for control rats, 20-116 sequences for HM3Dq rats). In addition, the baroreflex effectiveness index (BEI) was calculated as the number of baroreflex sequences divided by the overall number of SBP ramps, representing the proportion of SBP ramps that produced a reflex response to PI.

SNA recordings in anesthetized rats and analysis

These experiments were conducted in *Th-cre* rats injected with AAV-hSyn-DIO-hM3D(Gq)-mCherry (N= 4 male, 6 female) and non-injected *Th-cre* rats as controls (N= 3 male, 4 female). Rats were initially anesthetized with isoflurane (2.5%) in pure oxygen. Once anesthetized, a tracheostomy was performed and rats were intubated and mechanically ventilated (rate: 60 cpm; tidal volume: 1 mL/100gm)

with 2.0% isoflurane in pure oxygen. The right femoral artery and vein were exposed and cannulated with PE50 cannulas. The femoral artery cannula was connected to a pressure transducer calibrated using a sphygmomanometer to measure arterial BP. Urethane was administered via the femoral vein (1.3 g/kg, 10 % solution in sterile water, rate of infusion 0.2 mL/min), and then isoflurane was withdrawn. Adequate anesthesia was determined by the absence of a withdrawal reflex or pressor response to a firm tail or hind paw pinch. End-tidal CO_2 was measured using a capnograph (Columbus Instruments). The rate of ventilation was varied to achieve a table end tidal CO_2 of 3.0-3.5 %, which eliminated spontaneous breathing efforts. A paralyzing agent was not used. The splanchnic nerve was exposed using a dorsal retroperitoneal approach. The kidney and adrenal gland were retracted to expose the coeliac ganglion. The greater splanchnic nerve was isolated, placed on a recording electrode, and embedded in biocompatible silicone (Kwik-Cast, World Precision Instruments). The lumbar nerve was then exposed with a ventral approach. The intestines and the vena cava were retracted, and the lumbar sympathetic chain was isolated between the L2 and L3 ganglia, placed on a recording electrode, and embedded in biocompatible silicone Kwik-Cast (World Precision Instruments). Recording electrodes consisted of twisted Teflon-coated platinum-iridium bipolar wires (uncoated diameter: 0.005 inches, A-M systems, catalog # 777000). External wounds were closed with steel surgical clips. Hydration was maintained by infusion of 1mL/hour sterile saline for the duration of the experiment. After completion of surgery, a period of 30 minutes was allowed for stabilization of nerve recordings before proceeding with the experiment. At this point, intravenous boluses of phenylephrine (5 µg/kg in 0.1 mL) and sodium nitroprusside (5 µg/kg in 0.1 mL) were delivered to raise and lower BP to generate baroreflex function curves. After physiological parameters returned to baseline, CNO was administered i.v. (0.3mg/kg). Following 60 minutes of recording, phenylephrine and sodium nitroprusside were again delivered to raise and lower BP for baroreflex function curves. After data was acquired, rats were overdosed with urethane (30% of initial dose) followed by intracardial perfusion with fixative, or euthanasia using intravenous KCL (1 mL, 3M)

Physiological parameters were filtered and amplified (CWE Inc.) and then digitized with a CED 1401 A/D acquisition system using Spike2 (Version 9, Cambridge Electronic Design). BP was low-pass

filtered (200 Hz), amplified (x 500) and acquired at 500 Hz. End-tidal CO_2 was acquired at 200 Hz and calibrated using room air and 10% CO_2 mixed using mass flow controllers (Alicat). SNA was band-pass filtered (100 – 3,000 Hz), amplified (x20k or x50k), and digitized at 5 kHz. HR was derived from BP. For analysis, SNA was rectified and smoothed (time constant: 0.5 s), noise removed by subtracting the minimum activity observed following phenylephrine infusion, and normalized by dividing by the mean activity over a 10 s period preceding injections of CNO. Time course values for grouped data for SNA represent the mean of a 10 s period of activity extracted in 10 minute intervals for 1 hour after drug administration. Statistical comparisons of the change in SNA, MAP and HR between groups a 10 s period of activity data points 45 minutes after drug administration.

Baroreflex function curves were generated by plotting rectified and smoothed (time constant: 0.5 s) SNA against systolic pressure for each heart beat during ramp changes in BP induced by intravenous phenylephrine and sodium nitroprusside. Data points generated prior to and following CNO administration for each rat were normalized to the maximum and minimum value observed in the baseline condition. Boltzmann-sigmoid curves (equation below) were fitted to generate values for the top and bottom plateaus, V50 and slope for grouped comparisons.

$$Y = \text{Bottom} + \frac{\text{Top} - \text{Bottom}}{1 + e^{\frac{V50 - X}{Slope}}}$$

Respiratory recordings and analysis

Rats were placed in an unrestrained whole-body plethysmography chamber (Data Sciences International) with a continuous air flow of 2.5 L/min. Recording sessions were conducted between 9 am and 4 pm and lasted less than 6 h. The chamber was continuously perfused with room air generated by mass flow controllers operated by FlowVision software (Alicat Scientific). Rats were given 2 hours to acclimate to the chamber before CNO was administered (0.3 mg/kg, i.p.). Respiratory data represent the mean value of

100 consecutive breaths in quiescent state (sleep or quiet wakefulness), approximately 120 minutes after drug administration.

Metabolic measurements and analysis

Rats were placed in a plastic chamber (20 cm x 15 cm x 15 cm) connected to a Columbus Instruments Comprehensive Lab Animal Monitoring System with a continuous flow of 2 L/min of room air. Recording sessions were conducted between 9 am and 4 pm and lasted less than 6 h. Rats were given 2 hours to acclimate to the chamber before CNO was administered (0.3 mg/kg, i.p.). Metabolic data represents the mean value of 4 data points collected in 12 minute intervals approximately 120 minutes after drug administration.

Histology

Rats were deeply anesthetized with ketamine (150 mg/kg), xylazine (10 mg/kg), and acepromazine (2 mg/kg, i.m.) or urethane (see method for anesthetized recordings) and perfused transcardially with 4% paraformaldehyde in 100 mM phosphate buffer or pH-buffered 10% formalin. Brains were removed and post-fixed in the same fixative for 12-24 hrs. at 4°C. Brains were sectioned (30-50 μm) on a vibratome (VT-1000S, Leica Biosystems), and brain slices were stored in cryoprotectant at -20°C.

Immunohistochemistry was performed on free-floating sections at room temperature unless noted otherwise. Serial 1-in-6 sections were rinsed, then blocked in a solution containing 100 mM tris, 150 mM saline, 10% horse serum (v/v) 0.1% Triton-X (v/v) and incubated with primary antibodies for 60 min at room temperature then 4°C overnight. Sections were subsequently rinsed and then incubated with secondary antibodies for 60 min and rinsed again before mounting on slides. Slides were covered with ProLong Gold anti-fade mounting medium (P36931, Thermo Fisher Scientific).

Multiplex *in situ* hybridization was performed using RNAscope (V1 kit, Advanced Cell Diagnostics, Newark, CA). Serial 1-in-6 sections were washed in RNAase-free phosphate buffered saline,

mounted on charged slides, dried overnight, and processed according to the manufacturer's instructions. When necessary, immunohistochemistry was performed on the slide after the RNAscope procedure using antibodies against mCherry or CTB along with their respective secondary antibodies. Immediately following the RNAScope procedure, sections were rinsed and then incubated in blocking solution for 10 min followed by incubation in primary at room temperature for 60 min, rinsed and incubated in secondary antibodies for 30 min, rinsed and then dried overnight before cover slipping. Slides were cover slipped with ProLong Gold anti-fade mounting medium (P36931, Thermo Fisher Scientific).

Primary antibodies used include:

Chicken anti-GFP (1:1k, Aves Labs, catalog # GFP-1020, RRID: AB_10000240), mouse anti-TH (1:10k, MilliporeSigma, catalog # T1299, RRID: AB_477560), sheep anti-TH (1:1k, MilliporeSigma, catalog # AB1542, RRID: AB_90755), goat anti-ChAT (1:100, MilliporeSigma, catalog # AB144P, RRID: AB_2079751), goat anti-Phox2b (1:100, R&D Systems, catalog # AF4940, RRID: AB_10889846), rat anti-mCherry (1:4k, Thermo Fisher Scientific, catalog # M11217, RRID:AB_2536611), rabbit anti-DsRed (1:1k, Takara Bio, catalog # 632496, RRID: AB_10013483), goat anti-CTB (1:2k, List Biological Laboratories, catalog # 703, RRID: AB_10013220), rabbit anti-VMAT2 (1:5k, Phoenix Pharmaceuticals, catalog # H-V004, RRID: AB_2315577), guinea pig anti-VGLUT2 (1:2k, MilliporeSigma, catalog # AB2251-I, RRID: AB_2665454), rabbit anti-PNMT (1:5k, gift from M.C. Bohn, Northwestern University, Illinois, RRID: AB_2315181). Secondary antibodies were obtained from Jackson ImmunoResearch Laboratories, and used at 1:500 as follows: AlexaFluor-488 AffiniPure Donkey Anti-Chicken IgY (IgG) (H+L) (catalog #703-545-155, RRID: AB_2340375) AlexaFluor-488 AffiniPure F(ab')^2 Fragment Donkey Anti-Mouse IgG (H+L) (catalog #715-546-150, RRID: AB_ 2340849) Cy3 AffiniPure F(ab')^2 Fragment Donkey Anti-Mouse IgG (H+L) (catalog #715-166-150, RRID: AB_2340816), Cy3 AffiniPure Donkey Anti-Rabbit IgG (H+L) (catalog #711-165-152, RRID:AB_2307443). Information on antibody validation is available in The Antibody Registry (www.antibodyregistry.org) and manufacturers websites.

Fluorescent in situ hybridization probes

Th (Cat No. 314651), *Slc17a6*/VGLUT2 (Cat No. 317011), *Slc18a2*/VMAT2 (Cat No. 311971), *Slc32a1*/VGAT (Cat No. 424541) (Advanced Cell Diagnostics).

Cell counts and mapping

Neuronal mapping was conducted using Neurolucida software (MBF Bioscience, Williston, VT) with an AxioImager M2 microscope (Carl Zeiss). For brainstem sections, counting was performed on 1-in-6 series of sections that was subsequently aligned to Paxinos and Watson 7th edition. For the spinal cord, the cord was partitioned into cervical, thoracic, lumbar, and sacral blocks before sectioning. Histology was performed on sections from each region that were later localized to spinal segment based on similarity to Paxinos and Watson 7th edition.

Localization of spinally projecting neurons in the A5 region using CTB (for data in Fig. 1B and 8) and cFOS expression in the A5 region following CNO administration (for data Fig 2C) was assessed by counting cells on one side of the brain. Selectivity of DREADD expression (for data Fig 1C-D) was determined with bilateral counts. Cases in which fewer than 20% of the total population of A5 neurons were labeled (N=4 in total), and cases in which catecholaminergic neurons in the RVLM (i.e. C1 neurons) was greater than 5% of the total cells labeled (N=5 in total), were excluded from the analysis of the physiological effects of A5 stimulation.

Imaging

Digital images were acquired in grayscale using a Hamamatsu C11440 Orca-Flash 4.0LT digital camera (Hamamatsu). Max projections of z-stack images were exported (8-bit) and further image modifications were performed in Fiji software (27). Images were pseudo-colored and optimized for presentation, brightness and contrast was adjusted equally in all pixels of the image.

Statistics

Statistical comparisons were performed using Prism software (version 9.0, GraphPad). Following tests for normality (D'Agostino-Pearson or Shapiro-Wilk), tests for differences were performed as indicated in figure legends. Data are reported as mean ± SD unless otherwise noted and differences were considered significant when $p < 0.05$.

Results

Targeting A5 neurons in ventrolateral pons

We first assessed the distribution of A5 neurons, defined as neurons in the vlPons expressing detectable levels of TH (Fig. 1A), and determined the overlap of this population with spinally projecting neurons labeled with a conventional retrograde tracer injected bilaterally at T2-T3 in the spinal cord as well as the transcription factor Phox2b. Based on ipsilateral mapping of the A5 region in 3 rats, 73 ± 2 % of A5 neurons were spinally projecting, and 45 ± 10 % of spinally projecting neurons expressed TH (i.e. A5). Spinally projecting neurons lacking TH were located in the lateral pontine reticular nucleus. As previously reported (28), nuclear staining for Phox2b was weak or absent in most A5 neurons, whereas TH-negative neurons with strong nuclear expression of Phox2b were abundant in their immediate vicinity, especially in the caudal A5 region. Phox2b-expressing neurons in the caudal A5 region were located in the parasympathetic superior salivary nucleus (SSN) and the CO_2-sensing rostral retrotrapezoid nucleus (RTN) (28, 29). Spinally-projecting TH^-/ $Phox2b^+$ neurons were rare in the A5 region (7 of 973 neurons in 3 rats), however a small population of these cells was observed dorsally in the medial vestibular nucleus (Fig. 1A). This experiment confirms that the presence of TH along with projections to the spinal cord effectively distinguishes A5 neurons from most other cells in the A5 region.

We used this information to test the physiological effects of A5 neuron stimulation using an excitatory DREADD (HM3Dq) with intersectional recombinase-dependent targeting (Fig. 1B-E, Table 1). *Th-cre* rats were injected in the A5 region with AAV_2-FLEX-HM3Dq-mCherry (Fig. 1B), resulting in HM3Dq-mCherry expression in 55.7 ± 17.0 % of A5 neurons with a selectivity of 31.3 ± 9.8 %. Using

this approach, non-A5 neurons expressing HM3Dq-mCherry were principally located within the SSN region, many of which expressed Phox2b. Injections of a control virus (AAV_2-FLEX-mCherry, N=4) in the A5 region of *Th-cre* rats resulted in a similar pattern of mCherry expression and selectivity for A5 neurons (191 ± 34 mCherry+ neurons per rat, 32.4 ± 8.5 % of which express TH) that was comparable with injections of AAV_2-FLEX-HM3Dq-mCherry. Moreover, injection of AAV_2-FLEX-HM3Dq-mCherry in non-transgenic Sprague-Dawley rats lacking Cre resulted in minimal mCherry expression restricted at the site of injection (total bilateral count: 15-36 neurons per rat, N=3).

Although A5 neurons exhibited inconsistent Phox2b labeling, several studies have shown that the artificial Phox2b promoter PRSx8 effectively drives transgene expression in A5 cells (3, 9, 30). For this reason, we used a lentivirus driving Cre expression from the PRSx8 promoter co-injected with AAV_2-FLEX-HM3Dq-mCherry to label A5 neurons (Fig. 1C). This combination of viruses resulted in HM3Dq-mCherry expression in 41.8 ± 6.1 % A5 neurons with a selectivity of 27.5 ± 11.1 %. There was marked increase in the number of TH^-/$Phox2b^+$ neurons in these cases owing to labeling of neurons in the SSN and RTN (Fig 2A, B).

Given that A5 neurons represent the majority of spinally projecting neurons in the A5 region, we injected AAV_{rg}-Cre, a serotype of AAV with strong retrograde activity, in the spinal cord at T2-T3 and injected AAV_2-FLEX-HM3Dq-mCherry in the A5 region (Fig. 1D). This approach resulted in HM3Dq-mCherry expression in 49.3 ± 9.9 % of A5 neurons with a selectivity of 57.2 ± 18.4 %. With this approach, most TH^- neurons expressing HM3Dq-mCherry were located in the lateral pontine reticular nucleus.

In an attempt to improve the selectivity for A5, we used an intersectional targeting strategy to target spinally-projecting TH^+ neurons; AAV_{rg}-Flpo was injected in the spinal cord at T2-T3 and AAV_8-(Cre^{ON}/$Flpo^{ON}$)-HM3Dq-HA was injected in the A5 region *Th-cre* rats (Fig. 1E). This approach resulted in HM3Dq-HA expression in 65.4 ± 5.4 % of A5 neurons, and a selectivity of 53.9 ± 15.9 %. Labeling of catecholaminergic cells in the subcoeruleus and A7 groups increased using this approach. Injection of

AAV-(Cre^{ON}/Flpo^{ON})-HM3Dq-HA in non-transgenic Sprague-Dawley rats (N=3) resulted in no reporter expression.

Effect of A5 stimulation on BP and HR variability in anesthetized rats

We first established that activation of HM3Dq expressed in A5 neurons effectively increases cell activity by examining cFOS expression 90-120 minutes after administering the HM3Dq agonist Clozapine-N-oxide (CNO) (Fig. 2C). Intraperitoneal administration of CNO (0.3 or 1.0 mg/kg) significantly increased the number of A5 neurons expressing cFOS, while cFOS was undetectable in A5 neurons after administering 1.0 mg/kg CNO in *Th-cre* rats injected with AAV-FLEX-mCherry (Fig. 2C).

To test the effect of A5 stimulation on cardiovascular function in freely behaving rats, we injected CNO at a dose of 0.3 mg/kg (Fig. 3). Regardless of the targeting approach, activation of A5 neurons produced an elevation of BP that was evident compared to controls once the stress-response to handling had subsided (i.e. within 30 minutes after administered CNO), with the effect plateauing 90-180 minutes after CNO injection (Fig. 3A). The duration of the BP effect of A5 stimulation was long-lasting; BP typically returned to baseline after 6 hours, but in some cases remained elevated for > 8 hours. A5 stimulation caused bradycardia in some cases, but this effect was variable (Fig. 3B, D), only reaching statistically significant levels for the approaches using the PRSx8 promoter and spinal injection of AAV_{rg}-Cre to target A5 compared to controls administered CNO (Fig. 3D). We observed no significant change in pulse pressure with A5 stimulation in HM3Dq^{+} rats compared to controls (Table 2), suggesting no change in cardiac output. A5 stimulation also did not alter total locomotor activity during the first 3 hours after treatment during the inactive phase (Fig. 3E).

To link the BP effects observed in HM3Dq^{+} animals with activation of A5 neurons, we examined the relationship between the change in BP following CNO and both the efficiency and selectivity of A5 labeling with HM3Dq-mCherry. This analysis revealed a weak but significant positive correlation between the efficiency (Fig. 3F) and selectivity (Fig. 3G) of A5 labeling independent of the targeting approach and the increase in BP following CNO. By contrast, there was no correlation between the total

number of HM3Dq-labeled neurons (excluding A5 cells) and the increase BP following CNO (Pearson r= -0.03, R^2= 0.0, P=0.44). This suggests that activation of A5 neurons may be the determining factor in the magnitude of the BP effect observed in these experiments.

We conducted additional analysis to fully characterize the cardiovascular effects of A5 stimulation in *Th-cre* rats injected with AAV-FLEX-HM3Dq-mCherry or AAV-FLEX-mCherry. First, we utilized spectral analysis of heart rate variability (HRV) to assess cardiac autonomic balance during A5 stimulation (Fig. 4A-C). Frequency domain analysis of cardiac pulse interval showed the ratio of LF/HF was not different between groups (Fig. 4A), indicating no change in the balance of autonomic inputs to the heart (Fig. 4A). On the other hand, HR variance (Fig. 4D) and spontaneous baroreflex sensitivity (Fig. 4E) was elevated following CNO administration in $HM3Dq^+$ rats, but not $mCherry^+$ controls, suggesting that A5 stimulation sensitizes the cardiovagal baroreflex. Baroreflex effectiveness index was different between $HM3Dq^+$ rats and $mCherry^+$ controls, however there was no interaction between group and drug (saline vs. CNO) (Fig. 4F). To investigate diurnal influences on the cardiovascular effect of A5 stimulation we administered CNO during the dark phase (8pm-10pm) (Fig. 5A, B, Table 3). We found A5 stimulation significantly increased BP relative to saline injections regardless of the time of day, but the change in BP was smaller when CNO was administered during the active phase (lights off) when compared to the inactive phase (Fig. 5 A, Table 3). We also administered C21, an alternative agonist for HM3Dq, at a dose of 1 mg/kg, which resulted in a significant increase in BP in $HM3Dq^+$ rats, but not $mCherry^+$ controls, and no change in HR (Fig. 5C, D). Finally, we examined the BP effect of doses of CNO ranging from 0.01-1.0 mg/kg. CNO significantly increased BP compared to saline at doses $\leq$ 0.1 mg/kg (Fig. 5 E-F). To determine if sex-differences influences the BP effect of stimulating A5 neurons we compared the change in BP following A5 stimulation in male (N=15) and female (N=11) rats regardless of the targeting approach. There was no significant difference in the elevation in BP following A5 stimulation in male and female rats (14.4 ± 1.4 vs. 16.7 ± 2.0 mmHg, t=0.9711, df=24, P=0.34, Unpaired t-test).

412 **A5 neuron stimulation preferentially increases splanchnic sympathetic nerve activity**

413 To establish the effect of selective A5 stimulation on SNA, we recorded splanchnic and lumbar
414 SNA simultaneously in urethane-anesthetized mechanically-ventilated conditions (Fig. 6, Table 4).
415 Intravenous administration of CNO (0.3 mg/kg) resulted in a progressive increase in splanchnic SNA that
416 reached a plateau within 30 minutes and persisted for the duration of the experiment (approx. 3 hours)
417 (Fig. 6A-C). In contrast, lumbar SNA, MAP and HR was unchanged relative to control rats administered
418 CNO (Fig. 6A-C). We determined if A5 stimulation modulates the sympathetic baroreflex using
419 baroreflex function curves generated by intravenous boluses of phenylephrine and sodium nitroprusside to
420 raise and lower BP respectively (Fig. 6D, Table 5). A5 stimulation significantly increased the upper
421 plateau of the baroreflex function curve for splanchnic SNA, but other parameters were unchanged from
422 values prior to CNO administration. No change was observed in the lumbar nerve baroreflex function
423 curves (Fig. 6D, Table 5). Similar to what was observed with BP in freely-behaving rats (Fig. 3F), there
424 was a significant positive correlation between the efficiency of A5 neuron labeling and the elevation in
425 splanchnic SNA following CNO administration (Fig. 6E).

426

427 **A5 stimulation does not change ventilation or metabolic rate**

428 The respiratory effect of A5 stimulation was assessed with unrestrained whole body
429 plethysmography during the light phase (Fig. 7A). Administration of CNO (0.3 mg/kg) had no detectable
430 effect on breathing frequency or tidal volume in any group except when using the PRSx8 promoter to
431 target A5; in the latter group CNO produced a marked increase in tidal volume and total ventilation (Fig.
432 8B-D), likely caused by the activation of rostral RTN neurons (30) (Fig. 2B). There were also no
433 significant differences in the pattern of breathing (Fig. 7A) or the incidence of spontaneous sighs (Fig.
434 7E). Finally, stimulating A5 did not affect VCO_2, VO_2, or respiratory exchange ratio (RER) in any of the
435 groups tested (Table 6).

436

437 **A5 neurons with spinal projections also innervate brainstem regions regulating autonomic function.**

We assessed the brainstem projections of the bulbospinal A5 neurons using cases generated for physiology experiments in which A5 neurons were targeted with spinal injections of AAV_{rg}-Cre and labeled with AAV_2-FLEX-HM3Dq-mCherry as this approach yielded the highest selectivity for A5 neurons. In a separate series of rats, A5 neurons were targeted with spinal injections of AAV_{rg}-Cre and labeled unilaterally with an AAV driving Cre-dependent mGFP-2A-synaptophysin-mRuby that labels the cell body and axons of Cre-positive neurons with membrane tethered GFP, and putative synapses with synaptophysin-tethered mRuby. We used 2 cases in which the selectivity using AAV–FLEX-mGFP-2A-synaptophysin-mRuby was within the aforementioned range. Within the brainstem, the greatest density of A5 axonal labeling was observed in the dorsal vagal complex (nucleus of the solitary tract, NTS, and dorsal motor nucleus of the vagus, DMV) (Fig. 8A). The DMV was heavily innervated throughout its rostro-caudal extent with no apparent regional organization. Axonal labeling at caudal levels of the DMV appeared particularly dense owing to a large number of axons of passage that presumably innervate the spinal cord. A5 varicosities in the NTS were most apparent in the commissural region, but were evident throughout the nucleus. There was no innervation of the area postrema. We observed A5 varicosities in close apposition with cholinergic neurons in the nAmb (Fig. 8B-E). We observed numerous varicosities, many of which were $VMAT2^+$, in close apposition with the cell bodies and dendrites of $ChAT^+$ neurons in the external formation of the NAmb (Fig. 8B-D), according to the nomenclature of Bieger and Hopkins (31). We also observed sparse innervation of the compact formation of the NAmb (Fig. 8E), and dense varicosities within the SSN (Fig. 8F). Conversely, there was no innervation of the hypoglossal (Fig. 8A), facial and trigeminal motor pools or any apparent connections with cholinergic interneurons neurons in the intermediate reticular formation (32)or ventromedial medulla (33). Collectively, this indicates that bulbospinal A5 neurons also innervate parasympathetic preganglionic neurons throughout the brainstem, while seemingly avoiding cholinergic interneurons and motor neurons.

Labeled A5 axons and varicosities were abundant in the ventrolateral medulla (VLM) spanning the entire region between the facial nucleus and spinal decussation (Fig. 8B, G). We evaluated putative contacts with $PNMT^+$ neurons (Fig. 8H-J) and $VMAT2^+$ neurons in the VLM (Fig. 8B). In both cases we

observed examples of close appositions between A5 varicosities and catecholaminergic neurons in the VLM, however these cells did not appear to be the principal target of A5 in this region. Close appositions were not observed with the $PNMT^+$ neurons or $VMAT2^+$ in the dorsal medulla.

In the pons, A5 neurons heavily innervated the lateral aspect of the central gray overlapping with A6 and Barrington's nucleus (Fig. 8J), and sparsely innervated the lateral parabrachial nucleus and ventral lateral periaqueductal gray. In the spinal cord, cholinergic preganglionic neurons in the intermediolateral cell column and intermediate gray matter (lamina 10) were the principal targets of A5, consistent with prior reports (3, 5). The terminals of A5 neurons were observed in association with sympathetic preganglionic neurons in the IML and lamina 10 throughout the spinal cord including at the sacral levels (Fig. 9). Where the IML was absent (upper cervical and lower lumbar), labeled axons and terminals were evident in lamina 10, and axons were evident in the lateral funiculus. We also observed sparse fibers in the superficial layers of the dorsal horn at all spinal levels and occasionally sparse labeling in the ventral horn.

A5 neurons also express markers for glutamatergic neurotransmission

We examined the expression of VMAT2, the CNS vesicular transporter for biogenic amines including dopamine, noradrenaline and serotonin, and VGLUT2, the vesicular transporter for glutamate, in spinally-projecting neurons in the vlPons (Fig. 10). Based on ipsilateral counts in 3 rats, VMAT2 was expressed in 92.2 ± 3.3 % of A5 neurons. Conversely, TH was expressed in 91.2 + 9.9 % of $VMAT2^+$ cells within the A5 region. Thus, essentially all A5 neurons identified by the presence of TH have detectable levels of VMAT2, and most neurons expressing VMAT2 in the vlPons are A5 neurons (Fig. 10A, E). Functional experiments using optogenetic stimulation of A5 neurons indicate that these cells might exert part of their effects via fast neurotransmitter release (9). Although a previous study failed to detect VGLUT2 mRNA in A5 neurons (34), we observed VGLUT2 mRNA in 28.5 + 3.3 % of A5 neurons, of which 94.1 + 5.2 % also expressed VMAT2 mRNA. VGLUT2 mRNA expression varied appreciably in A5 neurons; in A5 cells that expressed VGLUT2 mRNA, 67.1 ± 11.9 % had staining that

was comparable to adjacent $TH^-/VGLUT2^+$ neurons (Fig. 10A, E). In contrast, vesicular GABA transporter (VGAT) mRNA expression was never observed in A5 neurons (0 $VGAT^+$ cells in a sample of 516 TH^+ A5 neurons in 2 rats).

We examined the expression of VMAT2 and VGLUT2 mRNA in bulbospinal neurons in vlPons identified using conventional retrograde tracing in 3 rats. In this series, 75.0 ± 8.9 % of bulbospinal neurons in the vlPons expressed VMAT2 mRNA with 23.6 ± 3.9 % these $VMAT2^+$ cells also expressing VGLUT2 mRNA. Collectively, VGLUT2 mRNA was observed in 23.7 ± 2.5 % of all bulbospinal neurons in the vlPons, with 74.6 ± 9.6% of these cells also expressing VMAT2 mRNA (Fig. 10B, F). Next, using cases generated for projection mapping (Fig. 8 and 9), we examined $mCherry^+$ varicosities of A5 neurons in the spinal cord and brainstem for VGLUT2 and VMAT2 immunoreactivity (Fig. 10C, D, G). Based on 173 samples in the IML and lamina 10 from 4 rats, 73.0 ± 6.4% of $mCherry^+$ varicosities expressed VMAT2 alone, 10.2 ± 3.8% expressed VMAT2 and VGLUT2, and 4.6 ± 0.8% expressed VGLUT2 alone. Based on 168 samples from the DMV, NTS, and VLM from 4 rats, 80.4 ± 3.2% of $mCherry^+$ varicosities expressed VMAT2 alone, 5.8 ± 2.1% expressed VMAT2 and VGLUT2, and 1.5 ± 0.9% expressed VGLUT2 alone.

Discussion

This study demonstrates that activation of A5 neurons in freely behaving rats increases BP but has no detectable effect on breathing patterns, metabolic rate, and locomotor activity, and in anesthetized conditions, activation of A5 neurons increases splanchnic SNA, but has no detectable effect on lumbar SNA. Furthermore, A5 neurons innervate targets in the brainstem and spinal cord that contribute to the sympathetic regulation of BP, as well as parasympathetic preganglionic neurons in the DMV, NAmb, and SSN. Finally, roughly a quarter of A5 neurons express VGLUT2 mRNA, however VGLUT2 protein was rarely detected in the A5 terminals. The potent effect of A5 neurons on splanchnic SNA suggests that visceral vasoconstriction may mediate the increase in BP when these neurons are activated in unanesthetized conditions. Given these findings we propose that A5 neurons serve a specialized role in

cardiovascular regulation by providing a mechanism for redistributing blood flow from the splanchnic circulation to the brain, heart and skeletal muscle.

A5 neurons regulate BP and visceral sympathetic outflow: implications for cardiovascular function

Chemogenetic stimulation of A5 neurons in unanesthetized adult rats resulted in a long-lasting elevation in arterial BP in the range of 10-15 mmHg. This result contrasts with previous studies that have reported either hypotension or no BP response following A5 stimulation (see introduction for references). Several factors may account for this discrepancy. First, the cellular effects of microinjected stimulatory chemical agents like glutamate and NMDA are short-lived compared to DREADDs which may last for hours (for example see (35) and this study). Second, many previous experiments were conducted under anesthesia, which may mask the effects of A5 stimulation on BP. For example, urethane at a doses required for general anesthesia attenuates the pressor response to intravenous noradrenaline in rats (36), which could explain why, in this study, chemogenetic stimulation of A5 neurons in anesthetized rats did not increase BP despite a marked increase in splanchnic SNA. And third, microinjections of chemical agents stimulate non-A5 neurons in the A5 region that may also regulate BP. The same is true also to various degrees for each approach used to target A5 in this study. However, the use of an intersectional strategy in which A5 neurons are the common denominator amongst heterogeneous populations of stimulated neurons lessens the confounding influence of the moderate selectivity achieved with each approach in isolation. Notably, the increase in BP was comparable irrespective of targeting approach and there was a positive correlation between the efficiency and selectivity of targeting A5 and the increase in BP. Hence, the activation of A5 neurons is the most parsimonious interpretation for the increase in BP reported here.

Several mechanisms may contribute to the increase in BP following A5 stimulation. A5 stimulation intensely recruited baro-sensitive fibers in the greater splanchnic nerve which have a vasoconstrictor function (37), whereas lumbar SNA was unchanged. Based on previous reports (4, 18), we suggest that the elevation in splanchnic SNA caused by A5 stimulation leads to an increase in

mesenteric vascular resistance. The splanchnic circulation holds 30% of circulating blood volume (38) that can be rapidly mobilized to increase cardiac return and filling, hence regionally selective mesenteric vasoconstriction alone may be sufficient to raise BP. By contrast, A5 stimulation did not increase HR or pulse pressure at doses sufficient to increase BP, in fact, HR tended to be reduced. This along with previous evidence (18) indicates the elevation in BP observed after A5 stimulation may not require increased cardiac output. On the other hand, A5 stimulation sensitized the cardiac baroreflex and to a lesser extent the splanchnic sympathetic baroreflex, indicating that A5 neurons modulate the arterial baroreflex. This is consistent with A5 innervation of brainstem regions mediating the arterial baroreflex ((6, 39) and this study) and previous functional studies (4, 20). Another possibility is that A5 stimulation also causes systemic circulatory effects through adrenal release of catecholamines (40) and noradrenaline spillover from the mesenteric circulation (41). Collectively, our data along with previous reports support the view that the cardiovascular effects of A5 stimulation stems from a preferential activation of visceral sympathetic drive, and to a lesser extent changes in the central processing of the baroreflex. Further studies will be required to demonstrate that the elevation in splanchnic SNA driven by A5 neurons produces mesenteric vasoconstriction with sufficient intensity to raise BP in unanesthetized conditions.

Projection mapping in the current and previous work (3, 5) demonstrate that A5 neurons heavily target the IML and lamina 10, suggesting that SPN are the principal target of A5 neurons in the spinal cord. A5 innervation of SPN may not be indiscriminate considering skeletal muscle SNA (i.e. lumbar SNA) was unchanged following by A5 stimulation, though the absence of an effect in this case could reflect the summation of opposing inputs to skeletal muscle SPN. Nevertheless, our results indicate that A5 neurons preferentially stimulate visceral vasoconstrictor SPN. At a population level, the preferential regulation of visceral SNA differentiates A5 neurons from C1 neurons in the rostral VLM (42), which recruit splanchnic, renal and lumbar SNA with comparable efficiency when activated with optogenetics (43-45). Notably, A5 neurons are a well-characterized target of C1 neurons (46-48) and may serve as a mechanism to amplify the action of C1 neurons on visceral vasoconstrictor SPN.

Activating A5 neurons has no effect on breathing, metabolic rate, and locomotor activity

The activity and function of pontine noradrenergic neurons is intimately linked with behavioral arousal (49), which, in turn, is associated with an elevation BP, HR, ventilation and metabolic rate. A previous study showed that optogenetic stimulation of A5 neurons also causes arousal from sleep in rats (30), suggesting A5 neurons may stimulate forebrain arousal systems. However, in this study, A5 stimulation had no effect on locomotor activity, breathing and metabolic rate, which demonstrates that the cardiovascular effects of A5 stimulation are not secondary changes in these parameters, and suggests that the elevation in BP is not related to a change in arousal state. Nevertheless, A5 neurons innervate brain regions that influence arousal (6), metabolic rate (50)and respiration ((51), and this study) so it is possible that A5 neurons influence these functions in some capacity.

Connectivity and signaling properties of A5 neurons

A5 neurons have been proposed to serve as a central modulator of generalized autonomic function because they innervate sympathetic and parasympathetic preganglionic neurons and the NTS (52, 53). Notably, pseudorabies tracing studies indicate that A5 neurons innervate both sympathetic and parasympathetic preganglionic neurons for individual organs, such as the pancreas (53, 54) and heart (55-57). Our study builds on this framework by showing that spinally-projecting A5 neurons innervate parasympathetic preganglionic neurons in the DMV, NAmb and SSN. The precise targets of A5 neurons within the DMV and NAmb remain to be determined, but the inconsistent effect of A5 neuron stimulation on HR suggests that cardiovagal preganglionic neurons are not the principal target within these nuclei. Altogether, the evidence suggests that individual A5 neurons are positioned to directly, and perhaps simultaneously, regulate both sympathetic and parasympathetic inputs to visceral organs, and indicates that the function of A5 neurons is not limited to the regulation of blood pressure.

Given the high levels of TH, DBH, and VMAT2 expression in A5 neurons it is presumed that these cells release noradrenaline, which powerfully regulates the activity of sympathetic and parasympathetic preganglionic neurons (21, 22, 58-60). In addition, we show that roughly a quarter of A5

neurons also express VGLUT2 mRNA, which may have gone unnoticed in previous studies using less sensitive methods (34). The expression of VGLUT2 mRNA in a subset of A5 neurons is consistent with the presence of functionally distinct subpopulations of A5 neurons, as previously suggested (61). Moreover, the presence of VGLUT2 provides a mechanism that explains the short-latency burst in SNA generated by optogenetic stimulation of A5 (9). However, A5 varicosities immuno-positive for VGLUT2 were less common than expected based on VGLUT2 mRNA in A5 neurons, which may be attributed to low levels of VGLUT2 protein or the presence of a unique sub-population of A5 neurons that release glutamate in brain regions that were not examined. While further studies are needed to identify a functional role for VGLUT2 in A5 neurons, glutamate co-transmission has been reported in other monoamine systems including the locus coeruleus (62) and C1 neurons (63)providing a theoretical basis for the function of co-transmission in these neurons (64, 65).

Perspectives and Significance

In conclusion, this study demonstrates that stimulation of A5 neurons preferentially increases splanchnic sympathetic outflow and that activation of A5 neurons in freely-behaving adult rats is sufficient to increase systemic BP. A5 neurons receive inputs stress-activated regions of the forebrain (dorsomedial hypothalamus, amygdala and periaqueductal grey), as well as inputs from the nucleus of the solitary tract and C1 adrenergic neurons in the rostral ventrolateral medulla (6, 46, 66). Considering this, activation of A5 may be important for patterned recruitment of the sympathetic efferents during systemic hypoxia, pain, defense reactions and changes in arousal (67-69). Furthermore, aberrant A5 activity could underlie regionally-specific changes in SNA in rodent models of hypertension (70), for example, Ang-II-salt hypertension in rats is associated with elevated splanchnic SNA, a reduction in renal SNA, and no change in lumbar SNA (71). A5 neurons are potently inhibited by small systemic doses of alpha2-adrenergic agonists (14, 72), a class of anti-hypertensive drug that effectively reduces BP and SNA in humans. Yet A5 neurons are often overlooked in models describing the sympathetic control of BP in health and in hypertensive states. This study indicates an important role for A5 neurons in the control of

the splanchnic circulation and provides the technical foundation to determine the contribution of A5 to cardiovascular homeostasis and disease.

Acknowledgments

This work was supported by National Institutes of Health grant HL148004 to S.B.G.A., and American Heart Association grant (19POST34430205) to G.M.P.R.S.

Author contributions

S.B.G.A., J.C.N. and G.M.P.R.S. designed the research; S.B.G.A. and G.M.P.R.S. conducted all the physiological experiments and data analysis; D.S.S. performed histological preparations. S.B.G.A. and A.V. analyzed histology, H.W. and H.U.Z generate unpublished reagents, S.B.G.A, G.M.P.R.S., D.S.S. wrote the paper and approved the final version of the manuscript.

Materials, Data and Code availability

All materials and data reported in this paper will be shared by the lead contact upon request.

This paper does not report original code

Any additional information required to reanalyze the data reported in this paper is available from the lead contact upon request.

References

1. **Aston-Jones G, and Waterhouse B**. Locus coeruleus: From global projection system to adaptive regulation of behavior. *Brain Res* 1645: 75-78, 2016.
2. **Manger PR, and Eschenko O**. The Mammalian Locus Coeruleus Complex-Consistencies and Variances in Nuclear Organization. *Brain Sci* 11: 2021.
3. **Bruinstroop E, Cano G, Vanderhorst VG, Cavalcante JC, Wirth J, Sena-Esteves M, and Saper CB**. Spinal projections of the A5, A6 (locus coeruleus), and A7 noradrenergic cell groups in rats. *J Comp Neurol* 520: 1985-2001, 2012.
4. **Huangfu D, Hwang LJ, Riley TA, and Guyenet PG**. Splanchnic nerve response to A5 area stimulation in rats. *Am J Physiol* 263: R437-446, 1992.

5. **Loewy AD, McKellar S, and Saper CB**. Direct projections from the A5 catecholamine cell group to the intermediolateral cell column. *Brain Res* 174: 309-314, 1979.
6. **Byrum CE, and Guyenet PG**. Afferent and efferent connections of the A5 noradrenergic cell group in the rat. *J Comp Neurol* 261: 529-542, 1987.
7. **Erickson JT, and Millhorn DE**. Hypoxia and electrical stimulation of the carotid sinus nerve induce Fos-like immunoreactivity within catecholaminergic and serotoninergic neurons of the rat brainstem. *J Comp Neurol* 348: 161-182, 1994.
8. **Hirooka Y, Polson JW, Potts PD, and Dampney RA**. Hypoxia-induced Fos expression in neurons projecting to the pressor region in the rostral ventrolateral medulla. *Neuroscience* 80: 1209-1224, 1997.
9. **Kanbar R, Depuy SD, West GH, Stornetta RL, and Guyenet PG**. Regulation of visceral sympathetic tone by A5 noradrenergic neurons in rodents. *J Physiol* 589: 903-917, 2011.
10. **Koshiya N, and Guyenet PG**. A5 noradrenergic neurons and the carotid sympathetic chemoreflex. *Am J Physiol* 267: R519-526, 1994.
11. **Huangfu DH, Koshiya N, and Guyenet PG**. A5 noradrenergic unit activity and sympathetic nerve discharge in rats. *Am J Physiol* 261: R393-402, 1991.
12. **Li YW, and Dampney RA**. Expression of Fos-like protein in brain following sustained hypertension and hypotension in conscious rabbits. *Neuroscience* 61: 613-634, 1994.
13. **Guyenet PG**. Baroreceptor-mediated inhibition of A5 noradrenergic neurons. *Brain Res* 303: 31-40, 1984.
14. **Andrade R, and Aghajanian GK**. Single cell activity in the noradrenergic A-5 region: responses to drugs and peripheral manipulations of blood pressure. *Brain Res* 242: 125-135, 1982.
15. **Neil JJ, and Loewy AD**. Decreases in Blood-Pressure in Response to L-Glutamate Micro-Injections into the A5 Catecholamine Cell Group. *Brain Research* 241: 271-278, 1982.
16. **Close JM, Neil JJ, and Loewy AD**. Actions of N-methyl aspartate and its antagonist aminophosphonovalerate on the A5 catecholamine cell group in rat. *Brain Res* 249: 393-396, 1982.
17. **Loewy AD, Gregorie EM, McKellar S, and Baker RP**. Electrophysiological evidence that the A5 catecholamine cell group is a vasomotor center. *Brain Res* 178: 196-200, 1979.
18. **Stanek KA, Neil JJ, Sawyer WB, and Loewy AD**. Changes in regional blood flow and cardiac output after L-glutamate stimulation of A5 cell group. *Am J Physiol* 246: H44-51, 1984.
19. **Drye RG, Baisden RH, Whittington DL, and Woodruff ML**. The effects of stimulation of the A5 region on blood pressure and heart rate in rabbits. *Brain Res Bull* 24: 33-39, 1990.
20. **Maiorov DN, Wilton ER, Badoer E, Petrie D, Head GA, and Malpas SC**. Sympathetic response to stimulation of the pontine A5 region in conscious rabbits. *Brain Res* 815: 227-236, 1999.
21. **Yoshimura M, Polosa C, and Nishi S**. Multiple actions of noradrenaline on sympathetic preganglionic neurons of the cat studied in the spinal cord slice. *Prog Brain Res* 81: 181-190, 1989.
22. **Lewis DI, and Coote JH**. Excitation and inhibition of rat sympathetic preganglionic neurones by catecholamines. *Brain Res* 530: 229-234, 1990.
23. **Coote JH, Macleod VH, Fleetwood-Walker S, and Gilbey MP**. The response of individual sympathetic preganglionic neurones to microelectrophoretically applied endogenous monoamines. *Brain Res* 215: 135-145, 1981.
24. **Polosa C, Yoshimura M, and Nishi S**. Electrophysiological properties of sympathetic preganglionic neurons. *Annu Rev Physiol* 50: 541-551, 1988.
25. **Inokuchi H, Yoshimura M, Polosa C, and Nishi S**. Adrenergic receptors (alpha 1 and alpha 2) modulate different potassium conductances in sympathetic preganglionic neurons. *Can J Physiol Pharmacol* 70 Suppl: S92-97, 1992.
26. **Shi H, Lewis DI, and Coote JH**. Effects of activating spinal alpha-adrenoreceptors on sympathetic nerve activity in the rat. *J Auton Nerv Syst* 23: 69-78, 1988.

27. **Schindelin J, Arganda-Carreras I, Frise E, Kaynig V, Longair M, Pietzsch T, Preibisch S, Rueden C, Saalfeld S, Schmid B, Tinevez JY, White DJ, Hartenstein V, Eliceiri K, Tomancak P, and Cardona A**. Fiji: an open-source platform for biological-image analysis. *Nat Methods* 9: 676-682, 2012.
28. **Kang BJ, Chang DA, Mackay DD, West GH, Moreira TS, Takakura AC, Gwilt JM, Guyenet PG, and Stornetta RL**. Central nervous system distribution of the transcription factor Phox2b in the adult rat. *J Comp Neurol* 503: 627-641, 2007.
29. **Stornetta RL, Moreira TS, Takakura AC, Kang BJ, Chang DA, West GH, Brunet JF, Mulkey DK, Bayliss DA, and Guyenet PG**. Expression of Phox2b by brainstem neurons involved in chemosensory integration in the adult rat. *J Neurosci* 26: 10305-10314, 2006.
30. **Burke PG, Kanbar R, Viar KE, Stornetta RL, and Guyenet PG**. Selective optogenetic stimulation of the retrotrapezoid nucleus in sleeping rats activates breathing without changing blood pressure or causing arousal or sighs. *J Appl Physiol (1985)* 118: 1491-1501, 2015.
31. **Bieger D, and Hopkins DA**. Viscerotopic representation of the upper alimentary tract in the medulla oblongata in the rat: the nucleus ambiguus. *J Comp Neurol* 262: 546-562, 1987.
32. **Toor R, Sun QJ, Kumar NN, Le S, Hildreth CM, Phillips JK, and McMullan S**. Neurons in the Intermediate Reticular Nucleus Coordinate Postinspiratory Activity, Swallowing, and Respiratory-Sympathetic Coupling in the Rat. *J Neurosci* 39: 9757-9766, 2019.
33. **Ruggiero DA, Giuliano R, Anwar M, Stornetta R, and Reis DJ**. Anatomical substrates of cholinergic-autonomic regulation in the rat. *J Comp Neurol* 292: 1-53, 1990.
34. **Stornetta RL, Sevigny CP, and Guyenet PG**. Vesicular glutamate transporter DNPI/VGLUT2 mRNA is present in C1 and several other groups of brainstem catecholaminergic neurons. *J Comp Neurol* 444: 191-206, 2002.
35. **Alexander GM, Rogan SC, Abbas AI, Armbruster BN, Pei Y, Allen JA, Nonneman RJ, Hartmann J, Moy SS, Nicolelis MA, McNamara JO, and Roth BL**. Remote control of neuronal activity in transgenic mice expressing evolved G protein-coupled receptors. *Neuron* 63: 27-39, 2009.
36. **Brezenoff HE**. Cardiovascular responses to noradrenaline in the rat before and after administration of various anaesthetics. *Br J Pharmacol* 49: 565-572, 1973.
37. **Janig W**. Pre- and postganglionic vasoconstrictor neurons: differentiation, types, and discharge properties. *Annu Rev Physiol* 50: 525-539, 1988.
38. **Fink GD**. Arthur C. Corcoran Memorial Lecture. Sympathetic activity, vascular capacitance, and long-term regulation of arterial pressure. *Hypertension* 53: 307-312, 2009.
39. **Loewy AD, Marson L, Parkinson D, Perry MA, and Sawyer WB**. Descending noradrenergic pathways involved in the A5 depressor response. *Brain Res* 386: 313-324, 1986.
40. **Strack AM, Sawyer WB, Platt KB, and Loewy AD**. CNS cell groups regulating the sympathetic outflow to adrenal gland as revealed by transneuronal cell body labeling with pseudorabies virus. *Brain Res* 491: 274-296, 1989.
41. **Aneman A, Eisenhofer G, Olbe L, Dalenback J, Nitescu P, Fandriks L, and Friberg P**. Sympathetic discharge to mesenteric organs and the liver. Evidence for substantial mesenteric organ norepinephrine spillover. *J Clin Invest* 97: 1640-1646, 1996.
42. **Guyenet PG, Stornetta RL, Bochorishvili G, Depuy SD, Burke PG, and Abbott SB**. C1 neurons: the body's EMTs. *Am J Physiol Regul Integr Comp Physiol* 305: R187-204, 2013.
43. **Abbott SB, Stornetta RL, Socolovsky CS, West GH, and Guyenet PG**. Photostimulation of channelrhodopsin-2 expressing ventrolateral medullary neurons increases sympathetic nerve activity and blood pressure in rats. *J Physiol* 587: 5613-5631, 2009.
44. **Souza GMPR, Stornetta RL, Stornetta DS, Guyenet PG, and Abbott SBG**. Adrenergic C1 neurons monitor arterial blood pressure and determine the sympathetic response to hemorrhage. *Cell Rep* 38: 110480, 2022.

45. **Kanbar R, Stornetta RL, Cash DR, Lewis SJ, and Guyenet PG**. Photostimulation of Phox2b medullary neurons activates cardiorespiratory function in conscious rats. *Am J Respir Crit Care Med* 182: 1184-1194, 2010.
46. **Abbott SB, Kanbar R, Bochorishvili G, Coates MB, Stornetta RL, and Guyenet PG**. C1 neurons excite locus coeruleus and A5 noradrenergic neurons along with sympathetic outflow in rats. *J Physiol* 590: 2897-2915, 2012.
47. **Holloway BB, Stornetta RL, Bochorishvili G, Erisir A, Viar KE, and Guyenet PG**. Monosynaptic glutamatergic activation of locus coeruleus and other lower brainstem noradrenergic neurons by the C1 cells in mice. *J Neurosci* 33: 18792-18805, 2013.
48. **Malheiros-Lima MR, Silva TM, Takakura AC, and Moreira TS**. A5 noradrenergic-projecting C1 neurons activate sympathetic and breathing outputs in anaesthetized rats. *Exp Physiol* 107: 147-160, 2022.
49. **Berridge CW, Schmeichel BE, and Espana RA**. Noradrenergic modulation of wakefulness/arousal. *Sleep Med Rev* 16: 187-197, 2012.
50. **Cano G, Passerin AM, Schiltz JC, Card JP, Morrison SF, and Sved AF**. Anatomical substrates for the central control of sympathetic outflow to interscapular adipose tissue during cold exposure. *J Comp Neurol* 460: 303-326, 2003.
51. **Dobbins EG, and Feldman JL**. Brainstem network controlling descending drive to phrenic motoneurons in rat. *J Comp Neurol* 347: 64-86, 1994.
52. **Sved AF, Cano G, and Card JP**. Neuroanatomical specificity of the circuits controlling sympathetic outflow to different targets. *Clin Exp Pharmacol Physiol* 28: 115-119, 2001.
53. **Loewy AD, Franklin MF, and Haxhiu MA**. CNS monoamine cell groups projecting to pancreatic vagal motor neurons: a transneuronal labeling study using pseudorabies virus. *Brain Res* 638: 248-260, 1994.
54. **Jansen AS, Hoffman JL, and Loewy AD**. CNS sites involved in sympathetic and parasympathetic control of the pancreas: a viral tracing study. *Brain Res* 766: 29-38, 1997.
55. **Ter Horst GJ, Hautvast RW, De Jongste MJ, and Korf J**. Neuroanatomy of cardiac activity-regulating circuitry: a transneuronal retrograde viral labelling study in the rat. *Eur J Neurosci* 8: 2029-2041, 1996.
56. **Jansen AS, Wessendorf MW, and Loewy AD**. Transneuronal labeling of CNS neuropeptide and monoamine neurons after pseudorabies virus injections into the stellate ganglion. *Brain Res* 683: 1-24, 1995.
57. **Standish A, Enquist LW, Escardo JA, and Schwaber JS**. Central neuronal circuit innervating the rat heart defined by transneuronal transport of pseudorabies virus. *J Neurosci* 15: 1998-2012, 1995.
58. **Boychuk CR, Bateman RJ, Philbin KE, and Mendelowitz D**. alpha1-adrenergic receptors facilitate inhibitory neurotransmission to cardiac vagal neurons in the nucleus ambiguus. *Neuroscience* 193: 154-161, 2011.
59. **Martinez-Pena y Valenzuela I, Rogers RC, Hermann GE, and Travagli RA**. Norepinephrine effects on identified neurons of the rat dorsal motor nucleus of the vagus. *Am J Physiol Gastrointest Liver Physiol* 286: G333-339, 2004.
60. **Aiba I, and Noebels JL**. Adrenergic agonist induces rhythmic firing in quiescent cardiac preganglionic neurons in nucleus ambiguous via activation of intrinsic membrane excitability. *J Neurophysiol* 121: 1266-1278, 2019.
61. **Robertson SD, Plummer NW, de Marchena J, and Jensen P**. Developmental origins of central norepinephrine neuron diversity. *Nat Neurosci* 16: 1016-1023, 2013.
62. **Yang B, Sanches-Padilla J, Kondapalli J, Morison SL, Delpire E, Awatramani R, and Surmeier DJ**. Locus coeruleus anchors a trisynaptic circuit controlling fear-induced suppression of feeding. *Neuron* 109: 823-838 e826, 2021.

63. **DePuy SD, Stornetta RL, Bochorishvili G, Deisseroth K, Witten I, Coates M, and Guyenet PG**. Glutamatergic neurotransmission between the C1 neurons and the parasympathetic preganglionic neurons of the dorsal motor nucleus of the vagus. *J Neurosci* 33: 1486-1497, 2013.
64. **Svensson E, Apergis-Schoute J, Burnstock G, Nusbaum MP, Parker D, and Schioth HB**. General Principles of Neuronal Co-transmission: Insights From Multiple Model Systems. *Front Neural Circuits* 12: 117, 2018.
65. **Trudeau LE, and El Mestikawy S**. Glutamate Cotransmission in Cholinergic, GABAergic and Monoamine Systems: Contrasts and Commonalities. *Front Neural Circuits* 12: 113, 2018.
66. **Bajic D, Van Bockstaele EJ, and Proudfit HK**. Ultrastructural analysis of rat ventrolateral periaqueductal gray projections to the A5 cell group. *Neuroscience* 224: 145-159, 2012.
67. **Yardley CP, and Hilton SM**. The hypothalamic and brainstem areas from which the cardiovascular and behavioural components of the defence reaction are elicited in the rat. *J Auton Nerv Syst* 15: 227-244, 1986.
68. **Dampney RA**. Central neural control of the cardiovascular system: current perspectives. *Adv Physiol Educ* 40: 283-296, 2016.
69. **Guyenet PG**. Regulation of breathing and autonomic outflows by chemoreceptors. *Compr Physiol* 4: 1511-1562, 2014.
70. **Osborn JW, Fink GD, and Kuroki MT**. Neural mechanisms of angiotensin II-salt hypertension: implications for therapies targeting neural control of the splanchnic circulation. *Curr Hypertens Rep* 13: 221-228, 2011.
71. **Toney GM, Pedrino GR, Fink GD, and Osborn JW**. Does enhanced respiratory-sympathetic coupling contribute to peripheral neural mechanisms of angiotensin II-salt hypertension? *Exp Physiol* 95: 587-594, 2010.
72. **Byrum CE, Stornetta R, and Guyenet PG**. Electrophysiological properties of spinally-projecting A5 noradrenergic neurons. *Brain Res* 303: 15-29, 1984.

Figure 1. Identification and targeting of A5 neurons.

A) Distribution and co-localization of tyrosine hydroxylase (TH) and Phox2b immunoreactive neurons in relation to spinally projecting neurons labeled with cholera toxin B (CTB) in the ventrolateral pons. The A5 region was defined by the ventral border of the motor trigeminal nucleus, the medial edge of the superior olivary nuclei as depicted by the dashed-line box in B. B-E) Method (upper panel), distribution of labeled neurons (middle panel) and selectivity (lower panel) for the approaches used to target A5 neurons. In approach 1 (B), A5 neurons were targeted by injecting an AAV_2 driving cre-dependent expression of HM3Dq-mCherry in the A5 region of *Th-cre* rats. In approach 2 (C), A5 neurons were targeted by co-injecting a lentivirus driving cre expression from the Phox2a/b promoter PRSx8 and an AAV_2 driving cre-dependent expression of HM3Dq-mCherry in the A5 region. In approach 3 (D), A5 neurons were targeted by injecting a AAV_{rg}-cre in the thoracic spinal cord of outbred Sprague-Dawley rats and an AAV_2 driving cre-dependent expression of HM3Dq-mCherry in the A5 region. In approach 4 (E), A5 neurons were targeted by injecting a retrograde AAV_{rg}-Flpo in thoracic spinal cord of *Th-cre* rats and a AAV_8 driving cre- and flpo-dependent expression of HM3Dq-HA in the A5 region. Abbreviations: 5- trigeminal motor nucleus, 7n- Facial nerve, CG- central gray, me- mesencephalic trigeminal tract, py- pyramid tract, scp- superior cerebellar peduncle, SSN- superior salivatory nucleus, SO- superior olivary nucleus, vsc- ventral spinocerebellar tract. Scale bar: 100 μm in B, 200 μm for images in C-F

Figure 2. Distribution of HM3Dq-mCherry labeled neurons in the caudal A5 region and evidence for activation of A5 neurons following CNO administration.

A) HM3Dq-mCherry expression in the caudal A5 region when A5 neurons were targeted with the PRSx8 promoter. In these cases, HM3Dq expression was observed in $Phox2b^+$ neurons in the SSN and rostral retrotrapezoid nucleus (RTN). B) When A5 neurons were targeted with the PRSx8 promoter, expression of HM3Dq-mCherry co-localized with mRNA for Neuromedin B, a selective marker for RTN

chemoreceptor neurons. C) Administration of CNO drives cFOS expression in HM3Dq-mCherry+ A5 and non-A5 neurons in *Th*-cre rats. Administration of CNO in *Th*-cre rats injected AAV_2-FLEX-mCherry did not increase cFOS in $mCherry^+$ A5 neurons or non-A5 neurons. * P<0.05, **, ## P<0.01 vs. corresponding cell type in $mCherry^+$ + CNO group by Holm- Šídák's multiple comparisons test. Scale bar: 50 μm for all panels

Figure 3. A5 stimulation increases blood pressure.

A) Time course for mean arterial pressure (MAP) following administration of CNO (0.3 mg/kg, i.p.). B) Time course of heart rate (HR) following CNO. C, D) Grouped data for the change in MAP (C), HR (D) 120 minutes after administration of saline or CNO. There was a significant interaction between groups and the effect of CNO vs. saline on MAP ($F(4, 66) = 10.83$, $P< 0.0001$) and HR ($F(4, 66) = 3.233$, $P= 0.0175$) by two-way ANOVA. ** P<0.01, **** P<0.0001 vs. CNO in controls by Šídák's multiple comparisons test. E) Grouped data for sum of locomotor activity over 3 hours after administration of saline or CNO. There were no significant differences between groups by two-way ANOVA ($F(4,58) = 0.6635$, $P=0.62$). F, G) X-Y plots of transduction efficiency and selectivity for A5 neurons and the change in MAP.

Figure 4. Effect of A5 stimulation of time- and frequency-domain characteristics of heart rate.

A) Low frequency power of heart rate variability (HRV). There was no interaction between group and drug for $HM3Dq^+$ vs. $mCherry^+$ rats by two–way ANOVA ($F(1, 24) = 2.49$, $P=0.128$). B) High frequency power of HRV. There was no interaction between group and drug for $HM3Dq^+$ vs. $mCherry^+$ rats by two–way ANOVA ($F(1, 24) = 1.56$, $P=0.2232$). C) LF/HF ratio of HRV. There was no interaction between group and drug for $HM3Dq^+$ vs. $mCherry^+$ rats by two–way ANOVA ($F(1, 24) = 0.045$, $P=0.83$). D) HR variance. There was a significant interaction between group and drug for $HM3Dq^+$ vs. $mCherry^+$ rats by two–way ANOVA ($F(1, 24) = 7.80$, $P=0.01$), as well as a significant drug effect ($F(1, 24) = 5.86$, $P=0.02$) and group effect ($F(1, 24) = 10.72$, $P=0.003$). E) Spontaneous baroreflex sensitivity. There was a

significant interaction between group and drug for HM3Dq$^+$ vs. mCherry$^+$ rats by two–way ANOVA (F (1, 24) = 12.31, P=0.0018), as well as a significant group effect (F (1, 24) = 5.42. P=0.029). F) Baroreflex efficiency index (BEI). There was no interaction between group and drug for HM3Dq$^+$ vs. mCherry$^+$ rats by two–way ANOVA (F (1, 24) = 2.367, P=0.14), or drug effect (F (1, 24) = 1.014, P=0.32), but a significant group effect (F (1, 24) = 6.69, P=0.016). *** P<0.0001 for CNO in HM3Dq$^+$ vs. mCherry$^+$ rats by Šídák's multiple comparisons test.

Figure 5. Cardiovascular effects of A5 stimulation.

A, B) Effect of the time of day on changes in MAP (A) and HR (B) following CNO (0.3 mg/kg, i.p.). There was a significant interaction between the time of day and the effect of CNO vs. saline on MAP (F (1, 24) = 5.62, P= 0.026) and HR (F 1, 24 = 4.39, P= 0.047) by two-way ANOVA. **** P< 0.0001 vs. saline during same light phase, $^{\#\#}$ P<0.01 vs. CNO during the light phase, by Sidak's multiple comparisons test. C, D) Comparison of the cardiovascular effect of HM3Dq agonists CNO (0.3 mg/kg) and C21 (1 mg/kg) on the MAP (C) and HR (D). By unpaired t-test, the increase in BP was significantly greater in HM3Dq$^+$ than mCherry$^+$ rats for CNO (t=6.447, df=12, P<0.0001) and C21 (t=6.95, df=12, P<0.0001). There was no significant effect on HR in HM3Dq$^+$ vs. mCherry$^+$ rats for either drug (CNO, t=1.880, df=12, P=0.085; C21, t=0.75, df=12, P=0.47). **** P< 0.0001 vs. mCherry$^+$ with same drug. E, F) Dose-dependent effects of CNO on MAP (E) and HR (F). There was a significant dose-response relationship for the effect of CNO on MAP (F (2.76, 16.58) = 26.97, P<0.0001)), but not HR (F (2.33, 14.00) = 1.946, P=0.176) by repeated-measures one-way ANOVA with Geisser-Greenhouse correction. Dunnett's multiple comparisons test indicates that doses of CNO of 0.1 mg/kg or greater resulted in a significant increase in BP compared to saline. ** P<0.01, *** P<0.001 compared to saline. G, H) Time course of MAP (G) and HR (H) following administration of CNO at three doses (0.3 mg/kg, i.p.) and saline. Note the delayed increased in MAP after 0.1 mg/kg.

Figure 6. Effect of A5 stimulation on splanchnic and lumbar sympathetic nerve activity (SNA) in urethane anesthetized mechanically ventilated conditions.

A) Time course of splanchnic SNA (SSNA) and lumbar SNA (LSNA) and arterial BP (AP) following intravenous administration of CNO (0.3 mg/kg). B) Time course for the effect of CNO on splanchnic and lumbar SNA in $HM3Dq^+$ and control (no AAV injection) animals. C) Grouped data for the change in splanchnic SNA ($t=5.66$, $df=14$, $P<0.0001$, unpaired t-test), lumbar SNA ($U=30$, $P=0.92$, Mann Whitney test), MAP ($t=1.56$, $df=14$, $P=0.14$, unpaired t-test) and HR ($t=0.74$, $df=14$, $P=0.47$, unpaired t-test) in $HM3Dq^+$ and controls animals 45 minutes after administration of CNO. D) Sympathetic baroreflex function curves before and after CNO in $HM3Dq^+$ rats generate using non-linear regression (Boltzmann-sigmoid) on X-Y plots of MAP and splanchnic SNA or lumbar SNA generated using intravenous boluses of the pressor agent, phenylepherine, and depressor agent, sodium nitroprusside. Curves are normalized to the maximum and minimum value of integrated nerve activity prior to CNO administration. See table 5 for statistical comparisons. E) X-Y plots of the transduction efficiency for A5 neurons and the change in splanchnic SNA (Pearson $r = 0.80$, $R^2 = 0.64$, P (one-tailed) = 0.28) and lumbar SNA (Pearson $r = -0.03$, $R^2 = 0.0007$, P (one-tailed) = 0.47) in $HM3Dq^+$ rats.

Figure 7. Effect of A5 stimulation on resting ventilation in normoxia.

A) Traces of breathing following saline (left panel) and CNO (0.3 mg/kg, right panel) measured by unrestrained whole-body plethsymography. Downward deflections indicate inspiration. B) Grouped data for respiratory frequency following administration of saline and CNO. There was no significant effect of group ($F(1, 62) = 0.46$, $P=0.50$) or treatment ($F(4, 62) = 1.11$, $P=0.36$), and no interaction between group and treatment ($F(4,62)=0.45$, $P=0.77$) by two-way ANOVA. C) Grouped data for tidal volume following administration of saline and CNO. There was a significant group effect ($F(4, 62) = 5.18$, $P=0.0012$), but no significant of treatment effect ($F(1, 62) = 0.5639$ $P=0.46$) nor an interaction between group and treatment ($F(4, 62) = 2.27$, $P=0.072$). $^{*}P< 0.05$ vs. saline within-animal, $^{\#\#}P<0.01$ vs. CNO in controls by Šídák's multiple comparisons test. D) Grouped data for total ventilation following administration of

saline and CNO. There was a significant group effect (F (4, 62) = 6.69, P=0.0002), but no significant effect of treatment (F (1, 62) = 0.046, P=0.83), and a significant interaction between group and treatment (F (4, 62) = 4.29, P=0.004). * P< 0.05 vs. saline within-animal, ## P<0.01 vs. CNO in controls by Šídák's multiple comparisons test. E) Grouped data for sigh/augmented breath frequency following administration of saline and CNO. There was no significant group (F (4, 62) = 0.89, P=0.48) or treatment effect (F (1, 62) = 0.5198 P=0.47), and no interaction between group and treatment (F (4, 62) = 0.27, P=0.90) by two-way ANOVA.

Figure 8. Brainstem projections of A5 neurons.

A) Transverse sections of the dorsal vagal complex at three rostro-caudal levels. B) Transverse section of the ventrolateral medulla showing A5 innervation of cholinergic ($ChAT^+$ in blue) and catecholaminergic ($VMAT^+$ in blue) neurons. C) Max-projection Z-stack of the inset in B showing VMAT2 expression in mCherry varicosities that form close appositions (highlighted by arrows) with cholinergic neurons in the external formation of the NAmb. D) Max-projection Z-stack of a transverse section of a cholinergic neuron in the external formation of the NAmb (approx. bregma level: -14.00 mm) showing multiple putative synaptic contacts from A5 neurons labeled by spinal cord injection of AAVrg-Cre and injection in the A5 region of AAVDJ-hSyn FLEX-mGFP 2A synaptophysin-mRuby. Putative synapses indicated by co-localization of pseudo-colored GFP (magenta) and mRuby (green) highlighted by arrows. E) Transverse section of the rostral compact formation of the NAmb showing input from A5 neurons. F) Transverse section of the superior salivatory nucleus showing input from A5 neurons. G) Transverse section of the rostral VLM (RVLM) showing projections of A5 neurons labeled as per description in D. Synaptic contacts were abundant in the RVLM, with a minority of synapses forming close appositions with PNMT-positive C1 neurons. H-I) Putative synaptic contacts (highlighted by arrows) with PNMT-labeled dendrites. J) Transverse section of the locus coeruleus showing input from A5 neurons. Abbreviations- 7- Facial motor nucleus, 12- hypoglossal motor nucleus, cc- central canal, DMV- dorsal motor nucleus of the vagus, LRN- lateral reticular nucleus, me5- mesenphalic trigeminal nucleus, NAmb-

nucleus ambiguus, RVLM- rostral ventrolateral medulla, SSN- superior salivatory nucleus. Scale bar: 100 μm for A, B, E, F, H, J. 25 μm for C, D, H, I.

Figure 9. Spinal cord projections of A5 neurons.

A) Series of transverse sections of the spinal cord with ChAT labeling (upper panels) showing the location of images depicting projections of A5 neurons labeled with mCherry (panels i-x). A5 varicosities were observed in the vicinity of cholinergic neurons in the intermediolateral cell column (IML) and lamina 10. B-C) Montage of a coronal section from the thoracic spinal cord showing the close association between A5 projections and cholinergic sympathetic preganglionic neurons in the IML. Scale bar: 100 μm for all

Figure 10. Expression of vesicular monoamine transporter 2 (VMAT2) and vesicular glutamate transporter 2 (VGLUT2) in A5 neurons and spinal projecting neurons in the A5 region.

A) Image of a transverse section of the A5 region showing expression of VMAT2/*Slc18a2* and VGLUT2/*Slc17a6* mRNA in tyrosine hydroxylase expressing A5 neurons. White arrows indicate A5 neurons expressing VMAT2 but not VGLUT2 mRNA, yellow arrows indicate A5 neurons expressing VMAT2 and VGLUT2 mRNA B) Image of a transverse section of the A5 region showing expression of VMAT2/*Slc18a2* and VGLUT2/*Slc17a6* mRNA in spinally-projecting neurons labeled with CTB. White arrows: Spinally projecting neurons expressing VMAT2 but not VGLUT2 mRNA, yellow arrows indicate spinally projecting neurons expressing VMAT2 and VGLUT2 mRNA C) Max-projection Z-stack of a transverse section from the thoracic spinal cord showing the projections of A5 neurons (targeted with injections of AAV_{rg}-Cre in the spinal cord and labeled with AAV_2-FLEX-HM3Dq-mCherry), and immunostaining for VMAT2 and VGLUT2. D) High magnification single plane images taken from C showing the co-localization between mCherry-labeled varicosities and VMAT2 (magenta arrows), and rare triple-labeled varicosities expressing both VMAT2 and VGLUT2 (yellow arrows). E) Proportion of

A5 neurons (expressing TH) that co-localize with VMAT2 and/or VGLUT2. F) Proportion of spinally-projecting neurons (labeled with CTB) that co-localize with VMAT2 and/or VGLUT2. G) Proportion of mCherry-labeled varicosities in the spinal cord (left pie chart) and brainstem (right pie chart) that co-localize with VMAT2 and/or VGLUT2. Scale bars: A- 50 μm, B- 30 μm, C- 50 μm, D- 5 μm.

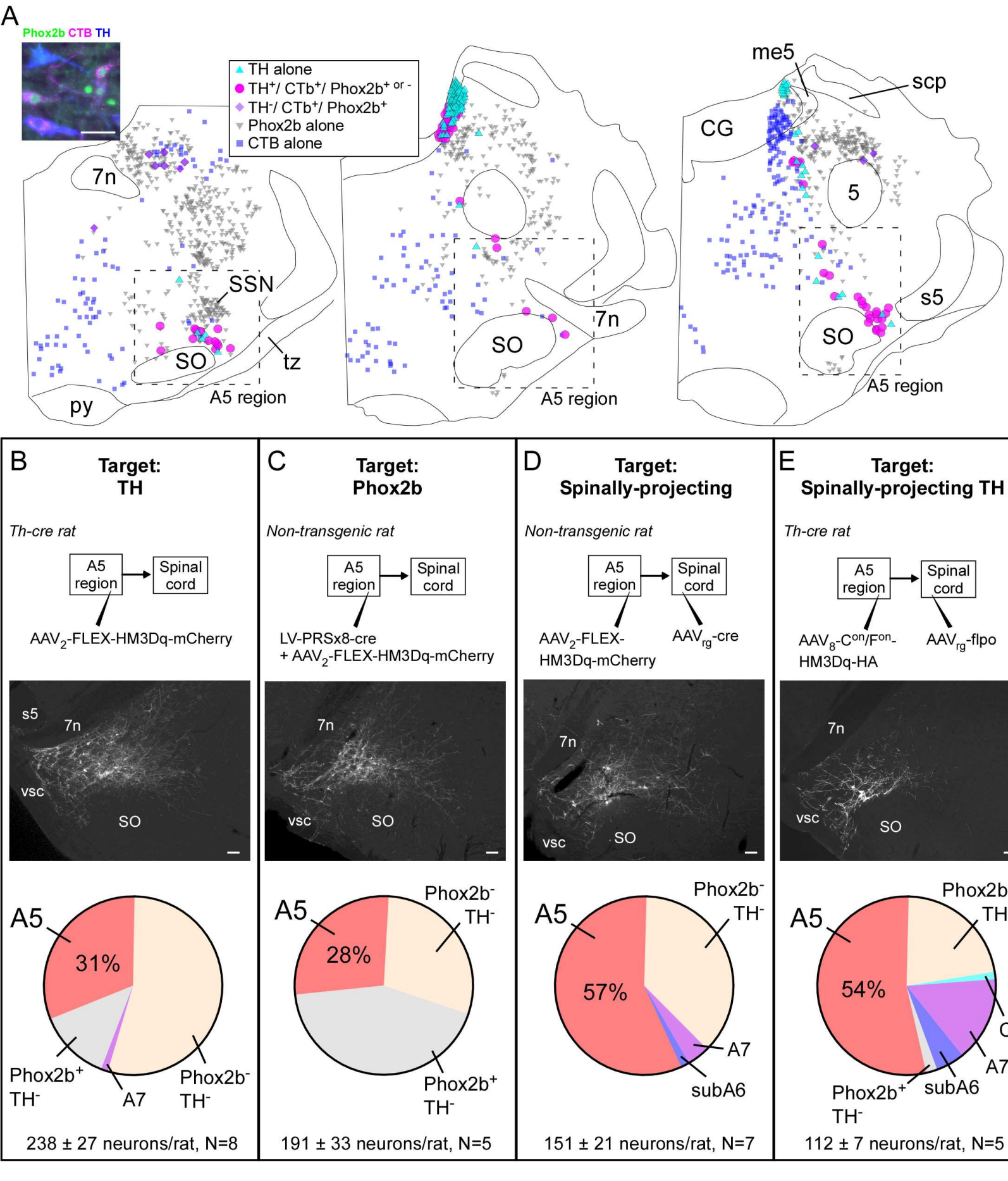

Figure 1

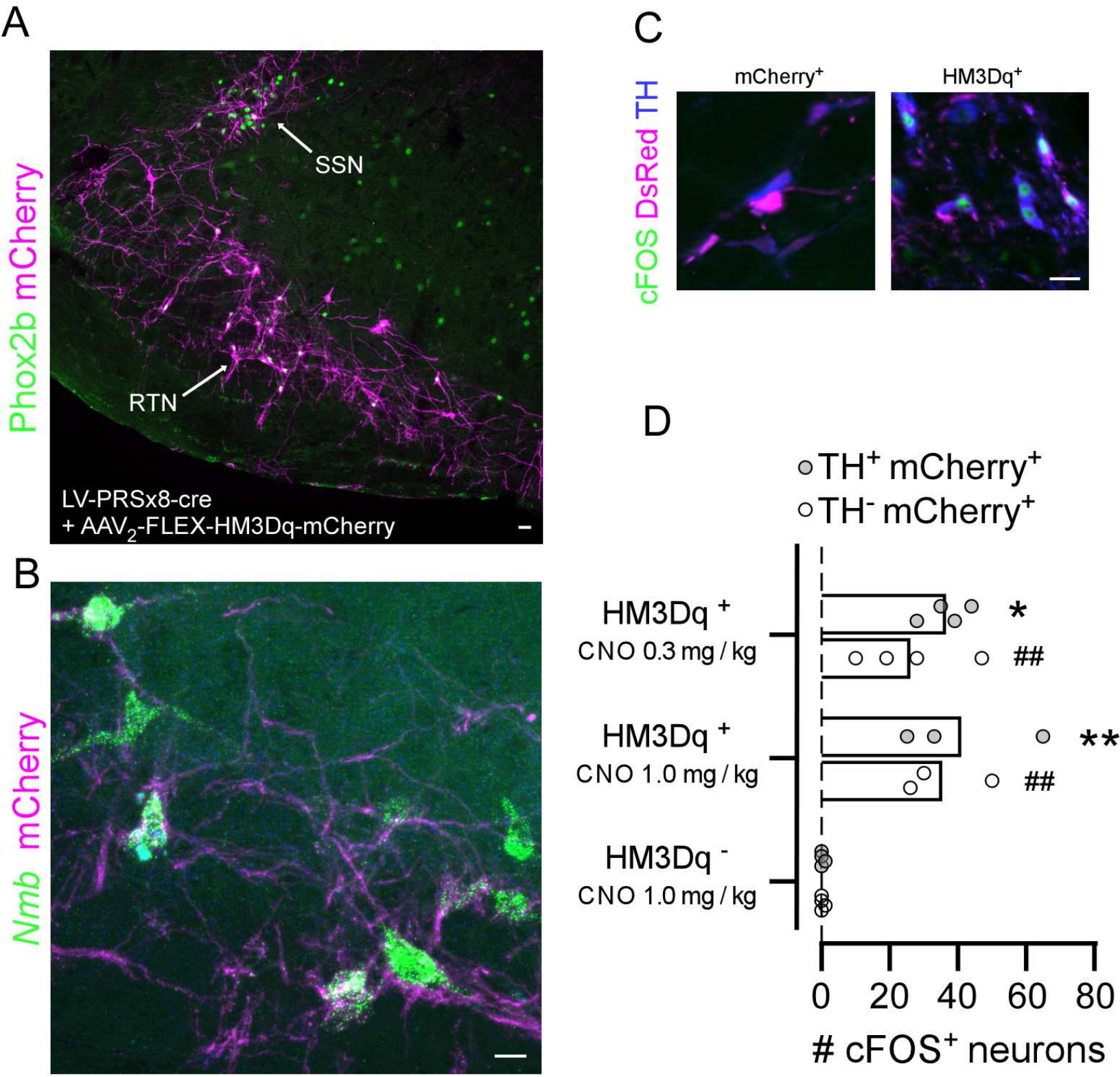

Figure 2

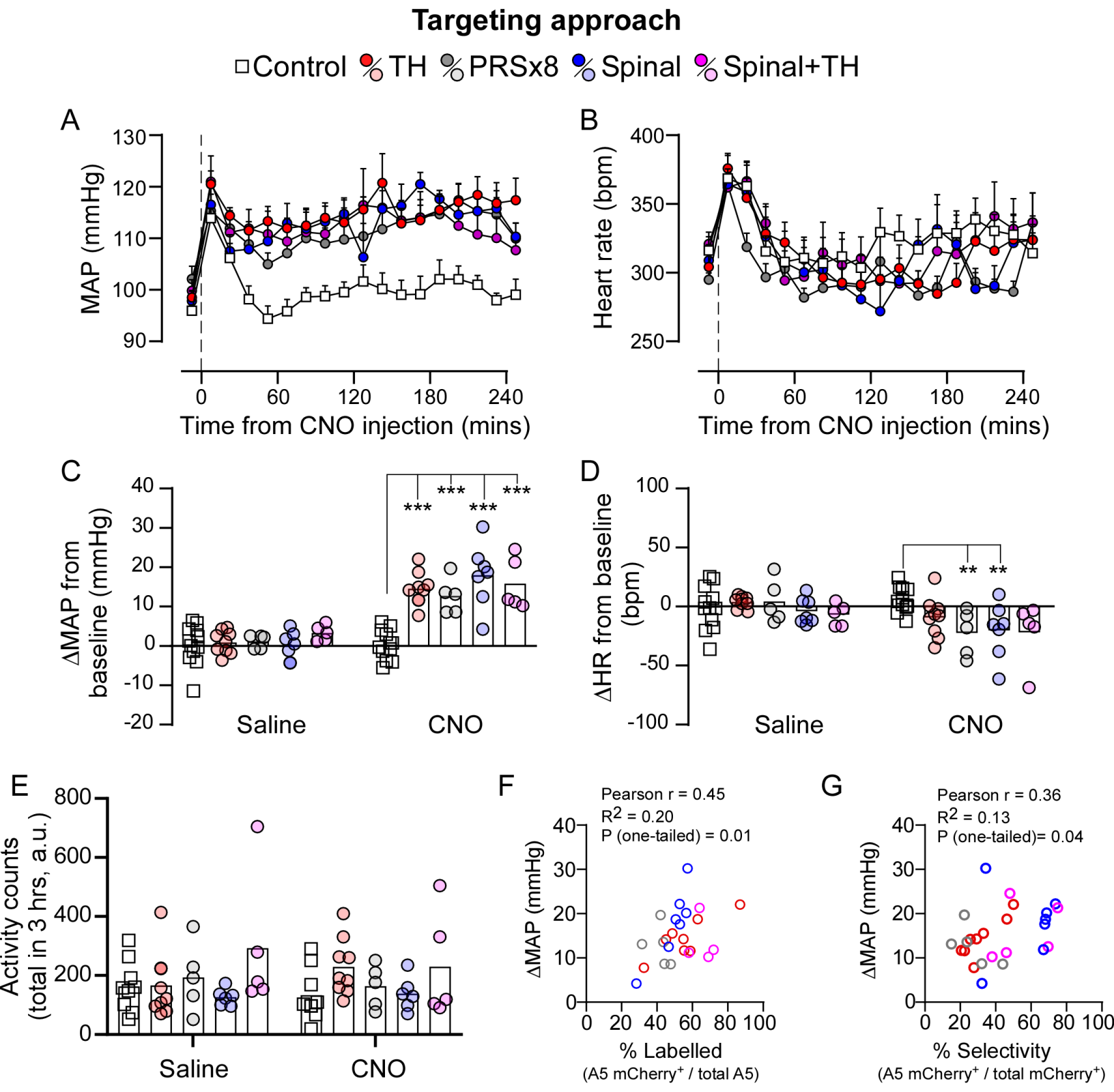

Figure 3

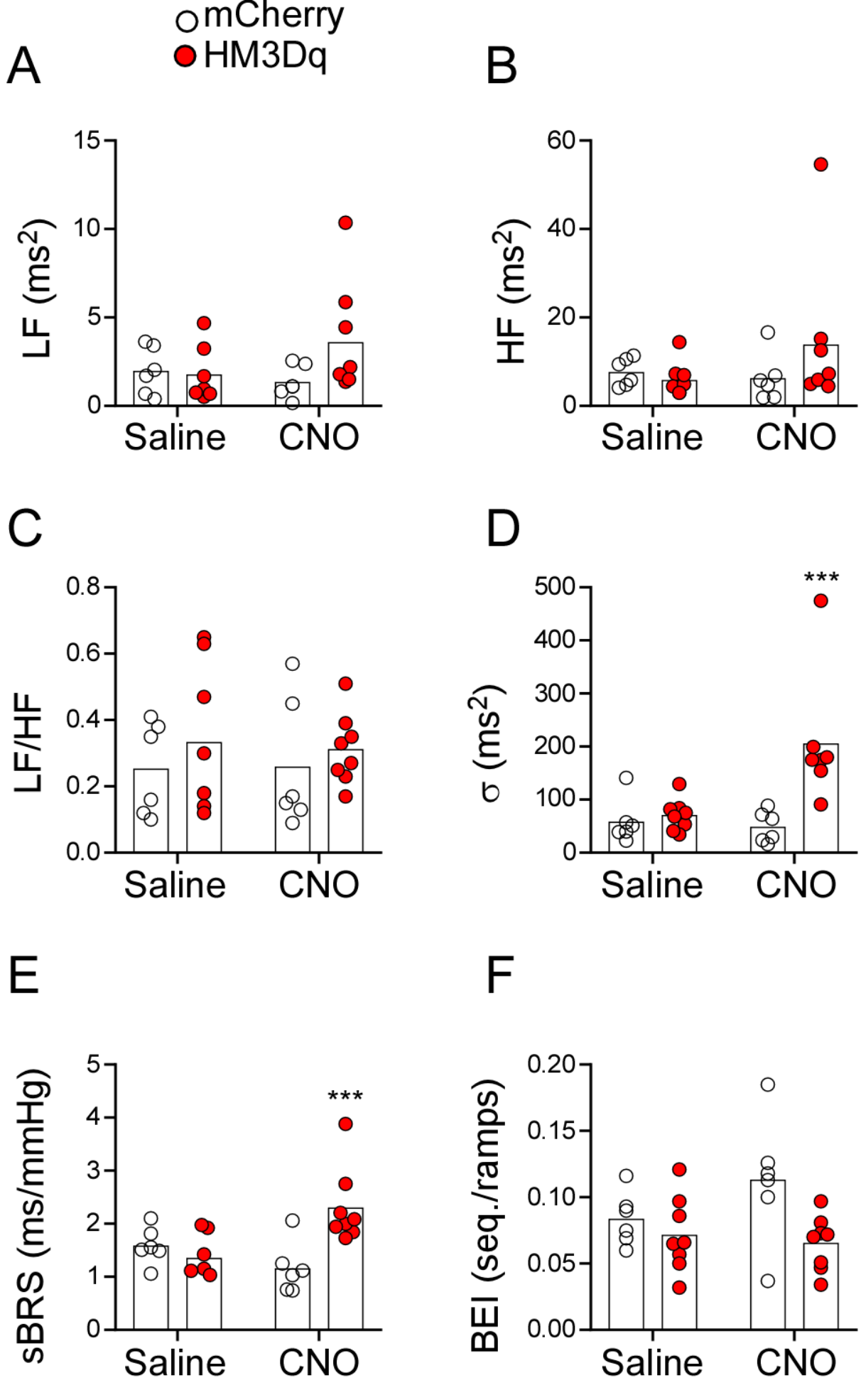

Figure 4

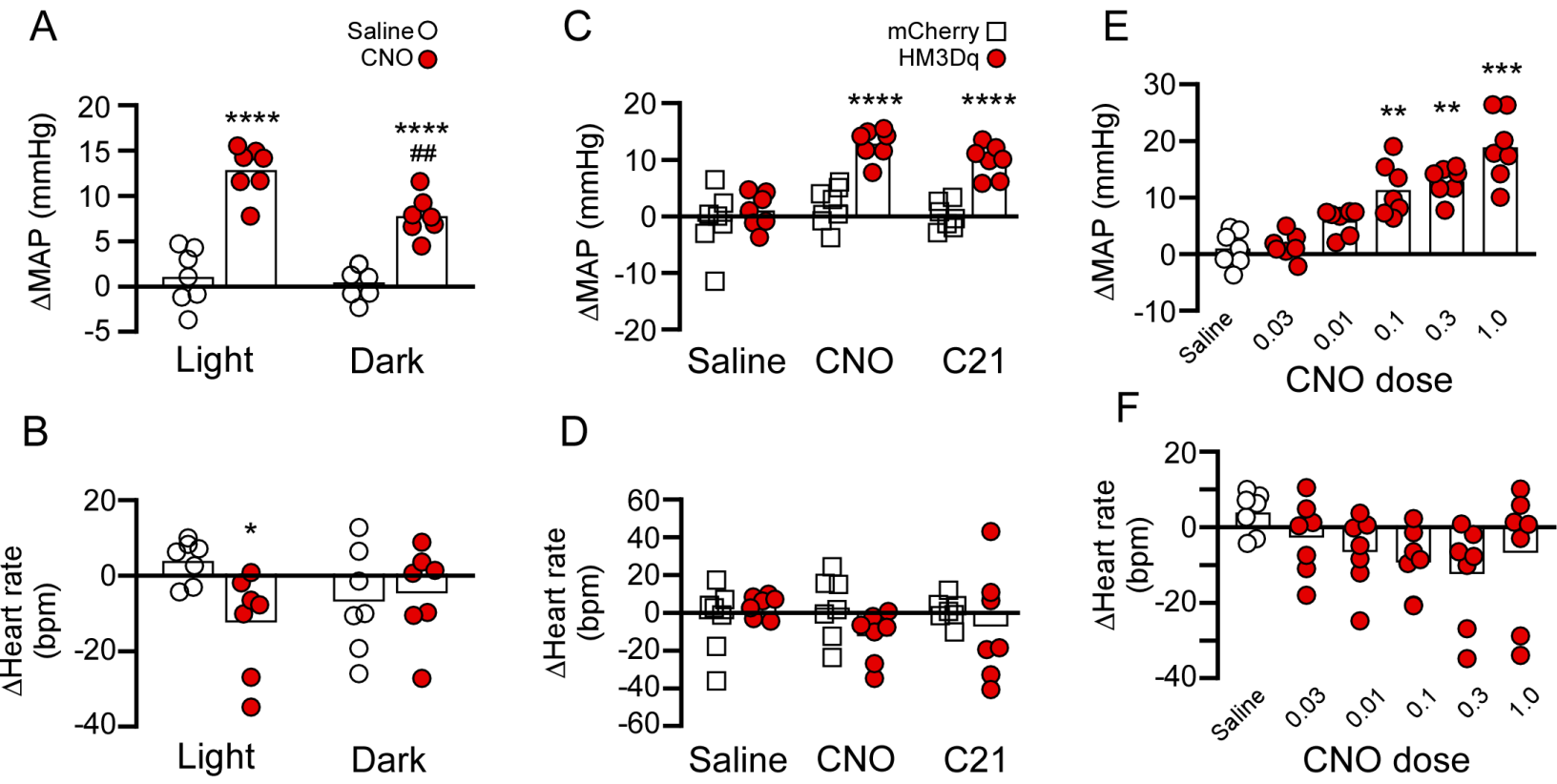

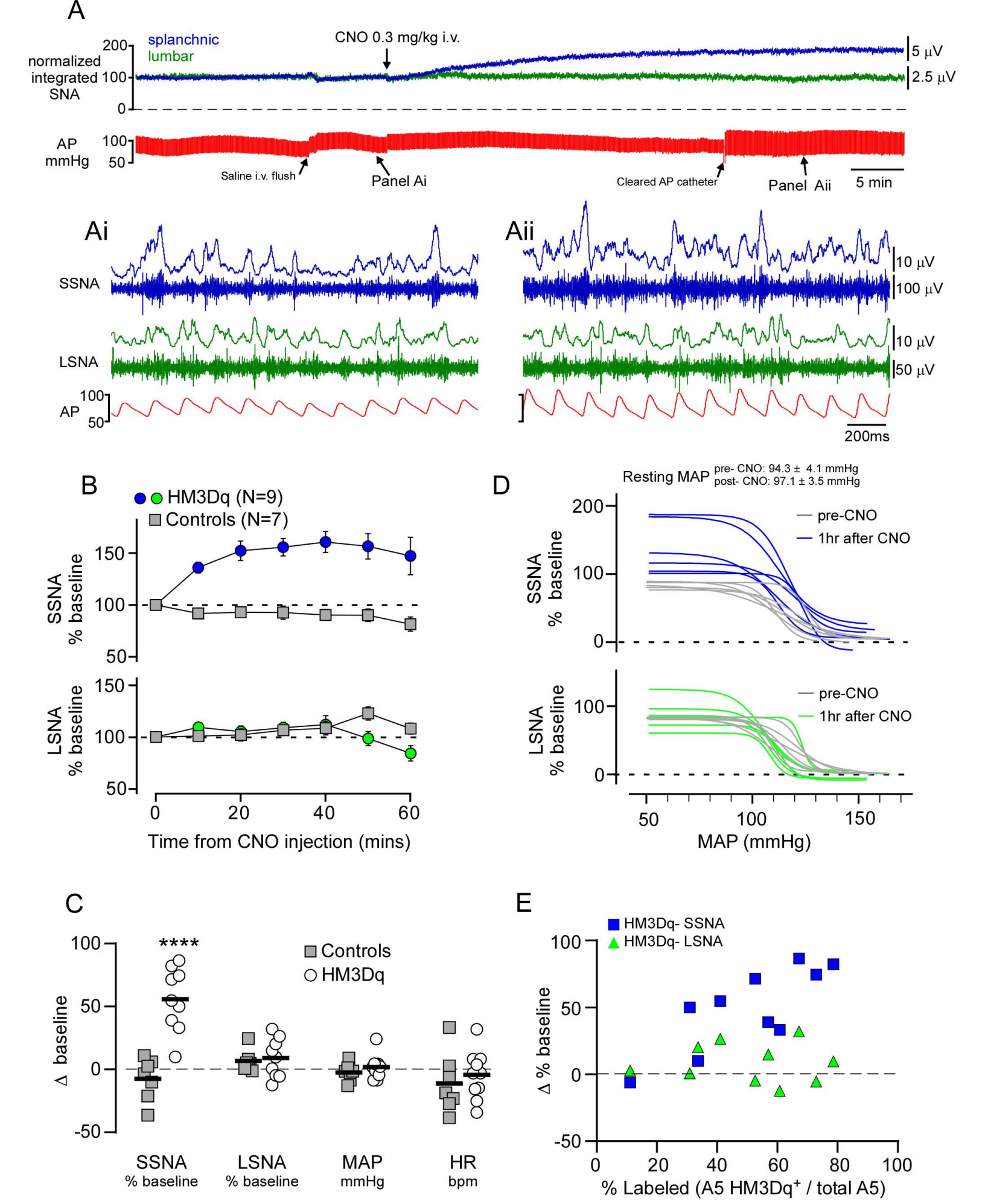

Figure 6

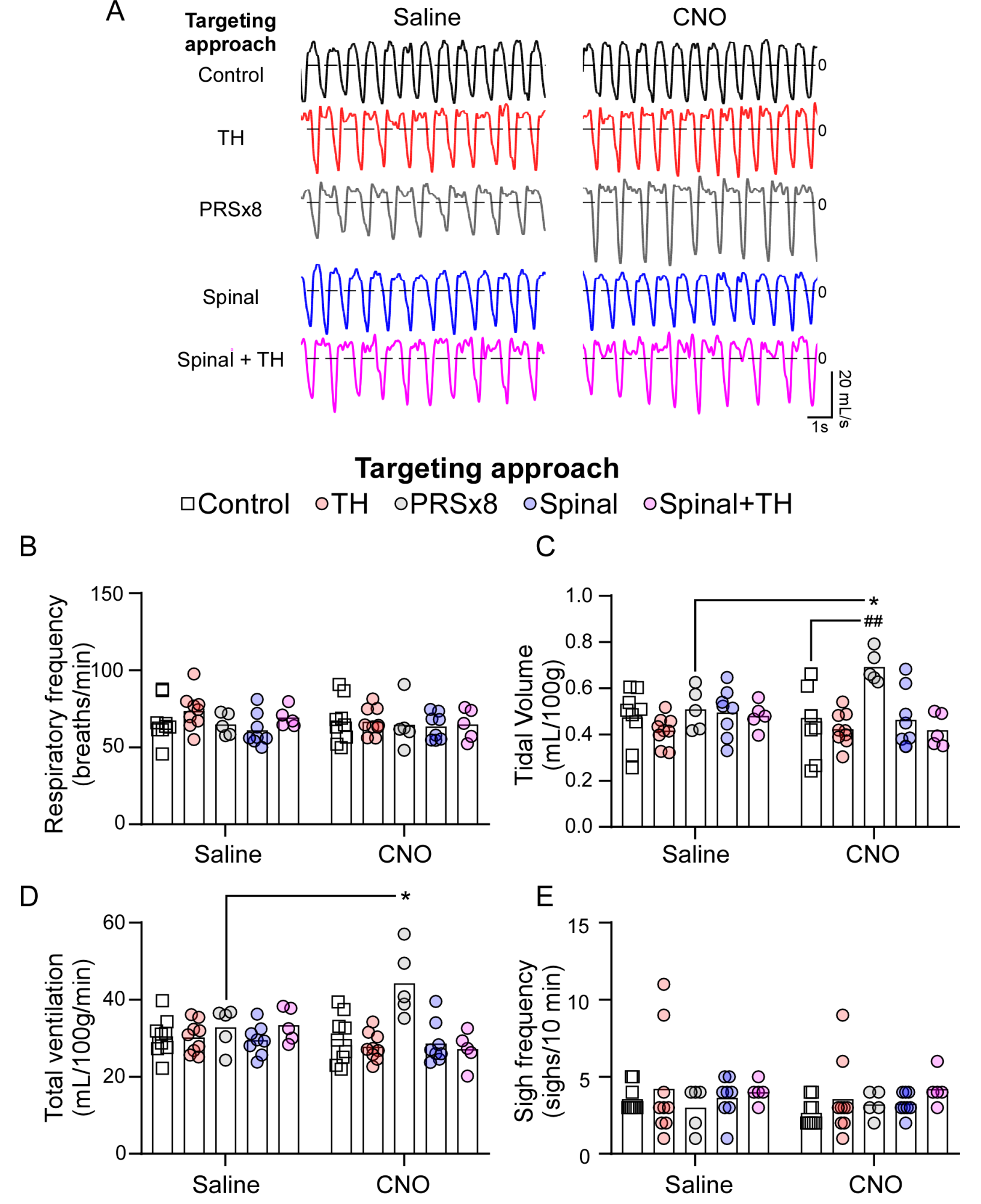

Figure 7

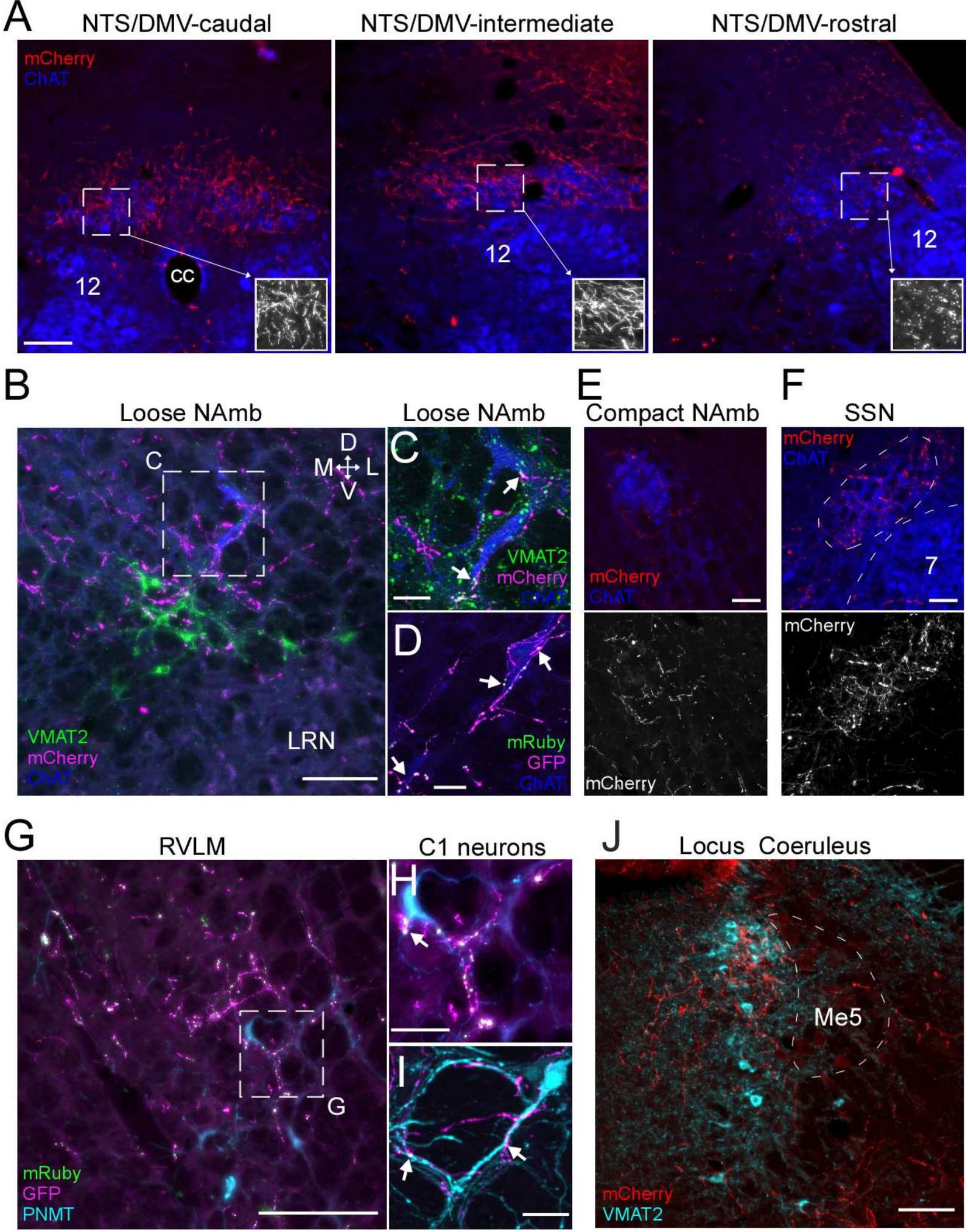

Figure 8

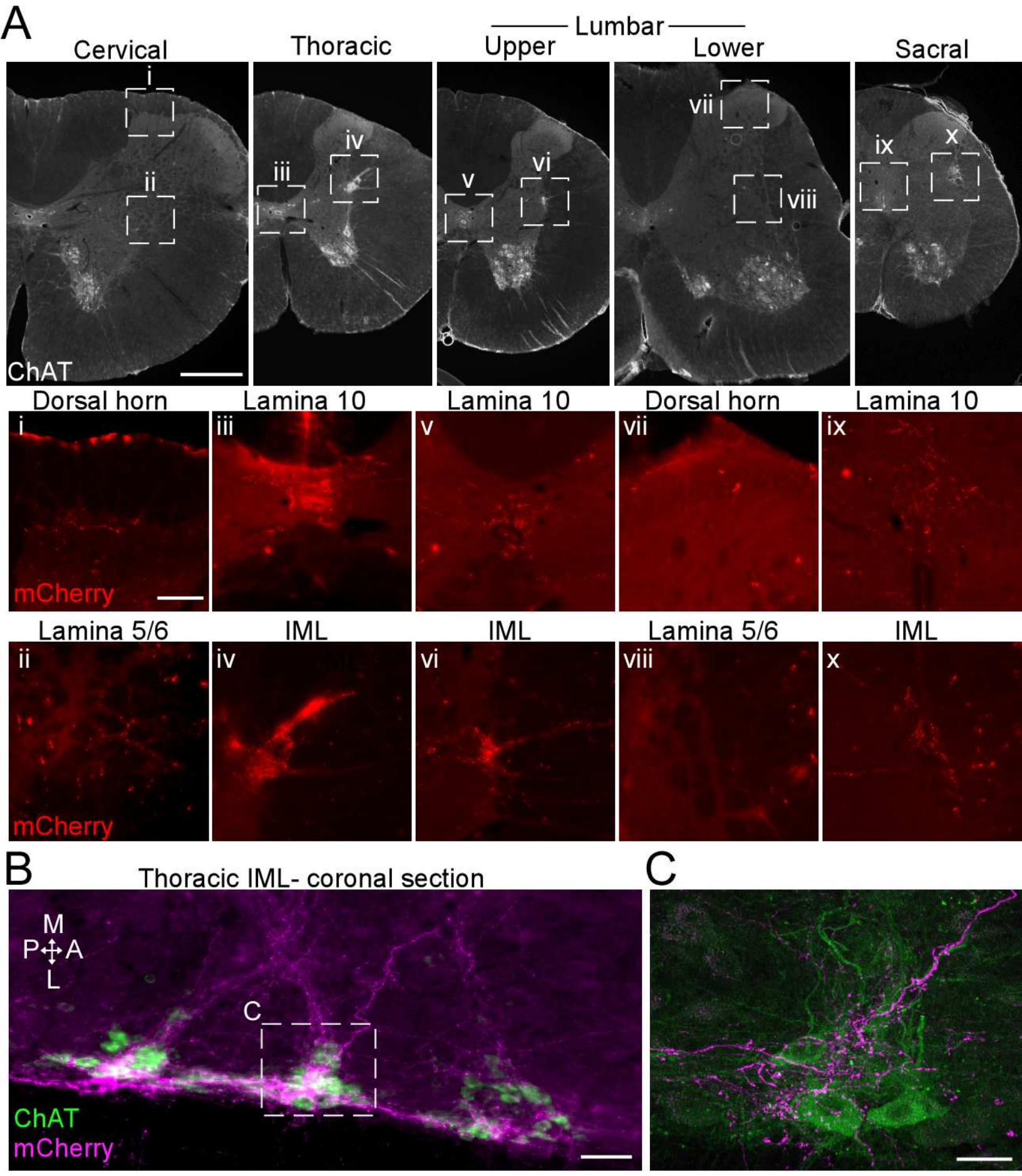

Figure 9

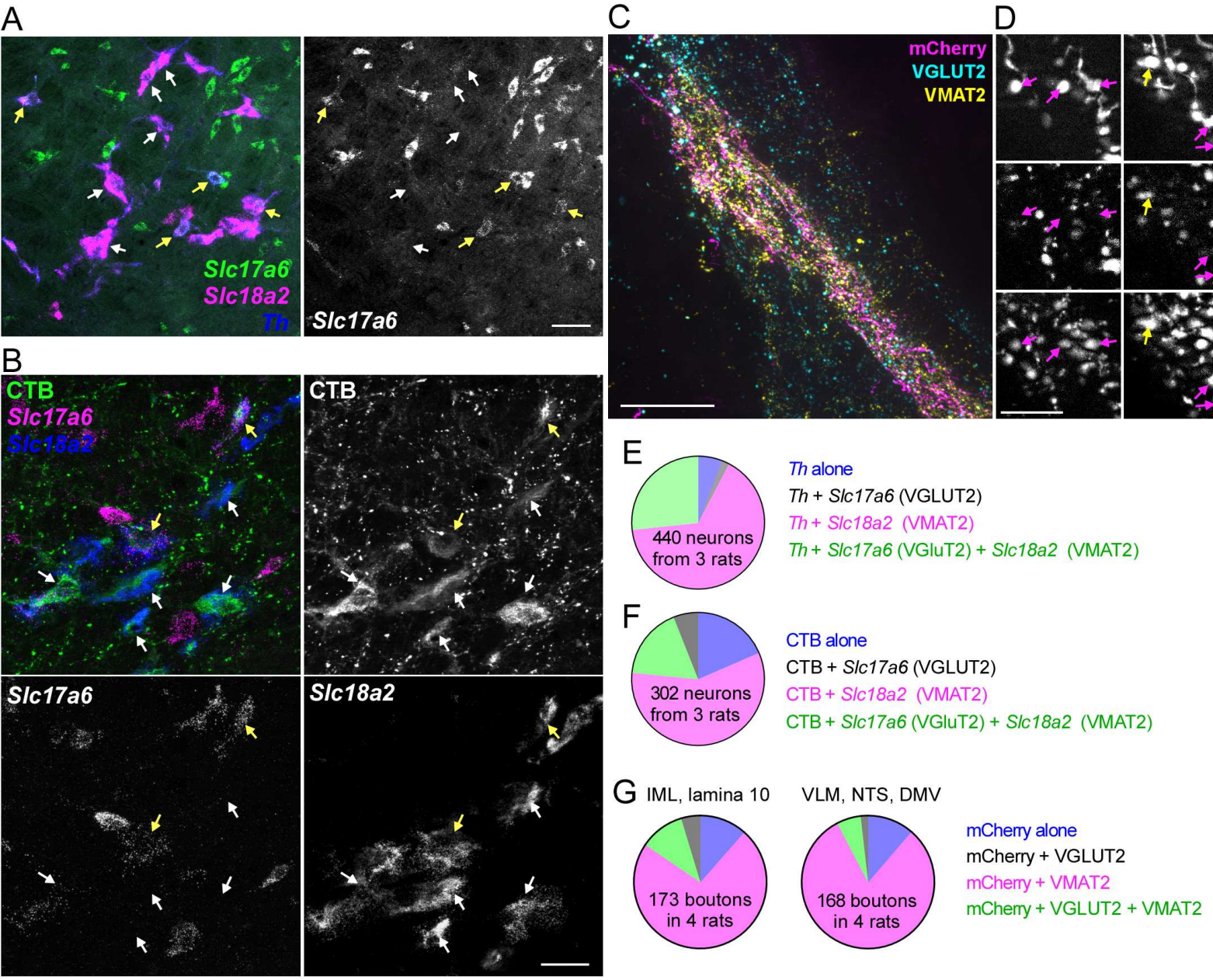

Figure 10

Table 1- Labelling of cells in the ventrolateral pons according to targeting model, related to figure 1.

Model	**A5**	**A6/subA6**	**A7**	**C1**	**Phox2b$^+$/TH$^-$**	**Phox2b$^-$ /TH$^-$**
1: TH N=8	28.5 (20.6-50.0)	0 (0-0)	0 (0-5.3)	0 (0-0)	12.3 (7.4-23.6)	58.2 (39.9-67.6)
2: PRSx8 N=5	23.8 (15.1-44.1)	0 (0-0)	0 (0-0)	0 (0-0)	49.7 (15.5-68.1)	26.6 (16.8-40.1)
3: Spinal N=7	67.2 (29.0-71.3)	0 (0-0)	0 (0-0)	0 (0-0)	2.2 (0.0-3.1)	30.1 (25.3-65.9)
4: Spinal + TH N=5	46.9 (36.5-74.1)	4.1 (0.0-12.2)	14.3 (10.4-21.4)	1.0 (0.0-3.5)	2.6 (0.7-3.1)	20.0 (10.3-31.6)

Values are quoted as % of total labelled neurons; values indicate median (min-max).

Table 2- Pulse pressure effect of A5 stimulation, related to figure 4.

		***Th*-cre /mcherry N=7**	***Th*-cre /HM3Dq N=7**
Pulse pressure (mmHg)	Saline	38.9 ± 6.0	37.1 ± 3.0
	CNO	40.2 ± 4.7	40.6 ± 2.6
Two-way ANOVA	Interaction- F (1, 24) = 0.50, P=0.49	Treatment- F (1, 24) = 2.11, P=0.16	Group- F (1, 24) = 0.21, P=0.66

Table 3- Absolute mean MAP and HR following injections of saline of CNO during the day or night

N=7	Saline AM	Saline PM	CNO AM	CNO PM
MAP, Pre-injection	98.7 ± 1.1 mmHg	107.4 ± 3.0 mmHg	98.4 ± 0.6 mmHg	109.0 ± 2.3 mmHg
MAP, post-injection	99.7 ± 1.4 mmHg	107.9 ± 2.5 mmHg	112.5 ± 1.8 mmHg ***	117.0 ± 2.3 mmHg ***
HR, Pre-injection	302.7 ± 30.7 bpm	380.4 ± 26.4 bpm	291.4 ± 25.9 bpm	378.8 ± 33.8 bpm
HR, post-injection	306.6 ± 30.5 bpm	373.6 ± 19.8 bpm	271.7 ± 16.4 bpm **	374.1 ± 35.8 bpm

** P<0.01, *** <0.0001 vs pre-injection values by Šídák's multiple comparisons test following two-way repeated measures ANOVA

Table 4- Baseline physiological parameters for anesthetized recordings of sympathetic nerve activity, related to figure 6.

	MAP mmHg		**HR bpm**		**etCO2 %**	
HM3Dq	100.2 ± 12.8	N=10	397.7 ± 41.1	N=10	3.4 ± 0.4	N=8
Control	97.5 ± 16.6	N=7	379.3 ± 48.1	N=7	3.3 ± 0.3	N=6
	t=0.3917, df=15, P= 0.70		t=0.8504, df=15, P=0.41		t=0.3213, df=12, P= 0.75	

Table 5- Boltzmann sigmoidal best-fit values for baroreflex curves in figure 6.

	sSNA N=6			lSNA N=6		
	Baseline	CNO	Paired t test	Baseline	CNO	Paired t test
Bottom %	2.0 ± 2.6	8.9 ± 13.1	t=1.38, df=5, P=0.23	1.4 ± 2.0	-1.7 ± 5.6	t=1.60, df=5, P=0.17
Top %	84.1 ± 4.9	137.1 ± 38.9	t=2.98, df=5, P=0.03	82.3 ± 1.3	87.3 ± 22.0	t=0.58, df=5, P=0.59
V50 mmHg	116.1 ± 6.4	116.2 ± 5.2	t=0.026, df=5, P=0.98	115.0 ± 6.1	111.1 ± 6.3	t=0.94, df=5, P=0.39

Slope %/mmHg	-8.5 ± 3.6	-7.5 ± 2.3	t=0.76, df=5, P=0.48	-7.1 ± 3.3	-4.8 ± 1.9	t=1.78, df=5, P=0.14

Table 6- Metabolic effects of A5 stimulation

		Controls, N=9	TH, N=8	PRSx8, N=5	Spinal, N=7
VO_2 mL/kg/h	saline	569 ± 120	615 ± 60	570 ± 95	555 ± 92
	CNO	627 ± 110	649 ± 109	616 ± 105	547 ± 95
Šídák's DF=50		t= 1.22, P= 0.64	t= 0.67, P= 0.94	t= 0.72, P= 0.92	t= 0.15, P= 0.99
VCO_2 mL/kg/h	saline	480 ± 103	538 ± 49	479 ± 92	464 ± 84
	CNO	529 ± 97	542 ± 91	517 ± 104	446 ± 76
Šídák's DF=50		t= 1.18, P= 0.67	t= 0.099, P= >0.99	t= 0.69, P= 0.94	t= 0.39, P= 0.99
RER	saline	0.84 ± 0.02	0.86 ± 0.04	0.84 ± 0.03	0.84 ± 0.04
	CNO	0.84 ± 0.03	0.83 ± 0.03	0.82 ± 0.02	0.82 ± 0.04
Šídák's DF=50		t= 0.038, P> 0.99	t= 1.68, P= 0.34	t= 0.78, P= 0.90	t= 1.14, P= 0.70

Table 7- Co-localization between TH, VMAT2 and VGLUT2 in spinally projecting neurons in the A5 region

Data set	Marker alone (%)	Marker + SLC17A6/VGluT2 (%)	Marker + SLC18A2/ VMAT2 (%)	Marker + SLC17A6/VGlut2 + SLC18A2 /VMAT2 (%)
Figure 9E Marker- TH	6.0 ± 2.2	1.7 ± 0.9	65.4 ± 0.3	26.8 ±1.7
Figure 9F Marker- CTB	75.0 ± 5.1	5.7 ± 0.9	18.0 ± 2.3	23.7 ± 1.5
Figure 9G, cord Marker- mCherry	12.3 ± 4.0	4.6 ± 0.8	73.0 ± 6.4	10.2 ± 3.8
Figure 9G, brainstem Marker- mCherry	12.4 ± 3.1	1.5 ± 0.9	80.4 ± 3.2	5.8 ± 2.1